Journal Pre-proofs

In vitro and *in vivo* studies of ocular topically administered NLC for the treatment of uveal melanoma

Cinzia Cimino, Elena Sánchez López, Angela Bonaccorso, Lorena Bonilla, Teresa Musumeci, Josefa Badia, Laura Baldomà, Rosario Pignatello, Agostino Marrazzo, Carla Barbaraci, María Luisa García, Claudia Carbone

PII: S0378-5173(24)00534-9
DOI: https://doi.org/10.1016/j.ijpharm.2024.124300
Reference: IJP 124300

To appear in: *International Journal of Pharmaceutics*

Received Date: 16 February 2024
Revised Date: 8 May 2024
Accepted Date: 31 May 2024

Please cite this article as: C. Cimino, E. Sánchez López, A. Bonaccorso, L. Bonilla, T. Musumeci, J. Badia, L. Baldomà, R. Pignatello, A. Marrazzo, C. Barbaraci, M. Luisa García, C. Carbone, *In vitro* and *in vivo* studies of ocular topically administered NLC for the treatment of uveal melanoma, *International Journal of Pharmaceutics* (2024), doi: https://doi.org/10.1016/j.ijpharm.2024.124300

Research article

In vitro and *in vivo* studies of ocular topically administered NLC for the treatment of uveal melanoma

Cinzia Cimino [a,b,c,d], Elena Sánchez López [c,e,f], Angela Bonaccorso [b,d], Lorena Bonilla [c,e], Teresa Musumeci [b,d], Josefa Badia [g,h,i], Laura Baldomà [g,h,i], Rosario Pignatello [b,d], Agostino Marrazzo [f,j], Carla Barbaraci [j, k], María Luisa García [c,e], Claudia Carbone [b,d,*]

[a] PhD in Biotechnology, Department of Biomedical and Biotechnological Sciences, University of Catania, Via Santa Sofia 97, 95123 Catania, Italy.

[b] Laboratory of Drug Delivery Technology, Department of Drug and Health Sciences, University of Catania, Viale A. Doria 6, 95124 Catania, Italy.

[c] Department of Pharmacy, Pharmaceutical Technology and Physical Chemistry, Faculty of Pharmacy and Food Sciences, University of Barcelona, 08028, Barcelona, Spain.

[d] NANOMED, Research Centre for Nanomedicine and Pharmaceutical Nanotechnology, University of Catania.

[e] Institute of Nanoscience and Nanotechnology (IN2UB), University of Barcelona, 08028, Barcelona, Spain.

[f] Unit of Synthesis and Biomedical Applications of Peptides, IQAC-CSIC, 08034, Barcelona, Spain.

[g] Department of Biochemistry and Physiology, Biochemistry and Biomolecular Science, University of Barcelona, 08028 Barcelona, Spain.

[h] Institute of Biomedicine of the University of Barcelona (IBUB), 08028 Barcelona, Spain.

[i] Research Institute Sant Joan De Déu (IR-SJD), 08950 Barcelona, Spain.

[j] Medicinal Chemistry Laboratory, Department of Drug and Health Sciences, University of Catania, Viale A. Doria 6, 95124 Catania, Italy.

[k] Present address: Laboratory of Medicinal Chemistry (CSIC Associated Unit), Faculty of Pharmacy and Food Sciences, and Institute of Biomedicine (IBUB), University of Barcelona, Av. Joan XXIII, 27-31, 08028 Barcelona, Spain.

***To whom correspondence should be addressed**

Claudia Carbone, PhD

Department of Drug and Health Sciences

University of Catania

Via Valdisavoia 5, 95123 Catania

E-mail: claudia.carbone@unict.it

Phone-Fax: +39 0957384251

Keywords: Lipid Nanoparticles; Ophthalmic delivery; Anti-inflammatory activity; HET-CAM test; Draize test; Fluorescent probe.

Abstract: Uveal melanoma is one of the most common and aggressive intraocular malignancies, and, due to its great capability of metastasize, it constitutes the most incident intraocular tumor in adults. However, to date there is no effective treatment since achieving the inner ocular tissues still constitutes one of the greatest challenges in actual medicine, because of the complex structure and barriers. Uncoated and PEGylated nanostructured lipid carriers were developed to achieve physico-chemical properties (mean particle size, homogeneity, zeta potential, pH and osmolality) compatible for the ophthalmic administration of (*S*)-(–)-MRJF22, a new custom-synthetized prodrug for the potential treatment of uveal melanoma. The colloidal physical stability was investigated at different temperatures by Turbiscan® Ageing Station. Morphology analysis and mucoadhesive studies highlighted the presence of small particles suitable to be topically administered on the ocular surface. *In vitro* release studies performed using Franz diffusion cells demonstrated that the systems were able to provide a slow and prolonged prodrug release. *In vitro* cytotoxicity test on Human Corneal Epithelium and Human Uveal Melanoma cell lines and Hen's egg-chorioallantoic membrane test showed a dose-dependent cytotoxic effect of the free prodrug on corneal cells, whose cytocompatibility improved when encapsulated into nanoparticles, as also confirmed by *in vivo* studies on New Zealand albino rabbits. Antiangiogenic capability and preventive anti-inflammatory properties were also investigated on embryonated eggs and rabbits, respectively. Furthermore, preliminary *in vivo* biodistribution images of fluorescent nanoparticles after topical instillation in rabbits' eyes, suggested their ability to reach the posterior segment of the eye, as a promising strategy for the treatment of choroidal uveal melanoma.

1. Introduction

Uveal melanoma (UM) is the most common malignant tumor of the inner eye, affecting 6 people per million every year and resulting in 50% mortality rate, mainly related to the development of liver metastasis (Kujala et al., 2003; Niederkorn et al., 2014). Occasionally, UM could affect ciliary body (7%) and iris (3%), but its main localization is in the choroid (90%) (Spagnolo et al., 2012). The achievement of the ocular tissues, and its posterior segment in particular, has always been a great challenge in the clinical field. In fact, for its complex structure and for the presence of several barriers and protection mechanisms, drug targeting to the inner eye results very difficult, both through systemic route and topical instillation. Systemic administration is usually inefficient because of the presence of the blood aqueous barrier, which protects the anterior region of the eye, and the blood-retinal barrier that protects the retina. On the other hand, the success of the topical instillation is limited by the presence of the tears and by blinking and drainage mechanisms, which are responsible of the short permanence time of the drug on ocular surface (1-2 minutes) (Ameeduzzafar et al., 2016; Natarajan et al., 2011). When the drug succeeds to reach the cornea, its permeation is strictly controlled by its lipophilicity (Sánchez-López et al., 2017). For the aforementioned reasons, only 2% of the administered drug is able to reach the inner eye through systemic route (Delplace et al., 2015), while for topical ophthalmic administration the percentage raises to 3-5% (Hughes et al., 2005). Aiming to directly target the inner eye, invasive methods are currently used in therapy, such as trans-scleral and intravitreal administrations. However, they possess low patient compliance and require highly qualified personnel (Thrimawithana et al., 2011). To reach the inner eye through topical administration, the encapsulation of drugs into delivery systems has demonstrated to be a successful strategy, which could be exploited using several carriers and modulating their properties in order to target specific areas of the eye. For instance, particle size influences nanoparticle permeation ability, while their superficial charge could favor interaction with mucin, improving the retention time on the ocular surface (Bonilla et al., 2021). Among the various carriers that could be employed for ophthalmic delivery, lipid nanoparticles – and nanostructured lipid carriers (NLC) in particular – demonstrated to be suitable for their biocompatibility and ability to act as a depot (Urtti, 2006), as well as for their high encapsulation efficiency, reduced drug loss and high stability during storage (Viegas et al., 2023). Several NLC systems demonstrated to be potentially useful in the treatment of eye posterior segment pathologies (De Oliveira et al., 2020; Platania et al., 2019), and the employment of fluorescent probes allowed to follow nanoparticles distribution after *in vivo* administration (Li et al., 2017).

Considering that the current therapy for UM only consists in surgery, radiation and enucleation (Rahmi et al., 2014), the development of novel drugs is the key for its actual cure. From the analysis of the biomolecular targets of this cancer, a new prodrug (*S*)-(–)-MRJF22 was synthetized esterifying haloperidol metabolite II (HP-mII) and valproic acid (VPA): the inhibition of histone deacetylase (HDACi) related to the VPA, and the σ_1-antagonism and σ_2-agonism attributable to HP-mII, resulted in a combined dual action, which was demonstrated to be promising as an adjuvant treatment for UM (Barbaraci et al., 2021). Aiming to achieve the inner eye, the encapsulation of this prodrug represents a potential strategy.

For these reasons, lipid nanoparticles and, specifically, nanostructured lipid carriers (NLCs) could constitute suitable carriers to encapsulate novel prodrugs such as (*S*)-(–)-MRJF22. Additionally, surface modification of NLC using PEGylation (P-NLC) or cationic compounds such as didodecyldimethylammonium bromide (DDAB, D-NLC), may be useful to reach posterior eye segment after topical administration. Indeed, cationic coating could favor interactions with the negatively charged mucin residues on the ocular surface (Razavi et al., 2022), while PEG is able to interpenetrate the mucin chains (Grassiri et al., 2021), providing, in both the situations, a prolonged residence of the carrier on the ocular surface.

Therefore, herein NLC, P-NLC and D-NLC were prepared and characterized in terms of particle size, homogeneity, zeta potential, pH and osmolality, and their stability was assessed using Turbiscan® Ageing Station. Moreover, NLCs morphology was analyzed through transmission electron microscopy (TEM) studies and their mucoadhesive properties were verified. (*S*)-(–)-MRJF22 was then successfully encapsulated and its release from the carriers was evaluated using Franz diffusion cells. NLCs cytocompatibility was confirmed both by *in vitro* cells (HCE-2 and 92-1) and HET-CAM (Hen's Egg Test on Chorioallantoic Membrane) tests and *in vivo* Draize tests. *In vivo* antiangiogenic capability and *in vivo* preventive anti-inflammatory properties were also investigated to confirm the prodrug therapeutical activity. Finally, the achievement of the posterior

segment of the eye was preliminary investigated through *in vivo* biodistribution images obtained after topical ophthalmic administration of the fluorescent nanosystems.

2. Materials and Methods

2.1 Materials

Kolliphor RH40 was provided by BASF Italia S.p.a. (Cesano Modena, Italy); Oleoyl Macrogol-6 Glycerides (Labrafil) was a gift from Gattefossé Italia s.r.l. (Milano, Italy); Hydrogenated Coco-Glycerides (Softisan 100) was bought from IOI Oleo GmbH (Oleochemicals, IOI group); Isopropyl myristate (IPM) was purchased from Farmalabor (Canosa di Puglia, Italy). Tris (hydroxymethyl)aminomethane buffer, methanol (MeOH) and ethanol (EtOH) were bought from Merck (Darmstadt, Germany). Didodecyldimethylammonium bromide (DDAB), Polyethylene Glycol 1500 (PEG 1500), Fluorescein isothiocyanate (FITC), phosphate buffer saline (PBS) components (NaCl, KCl, Na_2HPO_4, KH_2PO_4), artificial tear fluid (ATF) components ($CaCl_2 \cdot 2H_2O$, $NaHCO_3$, NaCl), mucin (mucin from porcine stomach type II), simulated tear fluid (STF) components (NaCl, $NaHCO_3$, $CaCl_2 \cdot 2H_2O$ and KCl), benzalkonium chloride, trypsin-EDTA (1X), 3-(4,5-dimethylthiazol-2-yl)-2,5-diphenyltetrazolium bromide (MTT), DMSO, DAPI (4',6-diamidino-2-phenylindole), sodium arachidonate, Hank's solution components ($CaCl_2 \cdot 2H_2O$, MgSO4, KCl, K_2HPO_4, $NaHCO_3$, NaCl, Na_2PO_4, glucose), paraformaldehyde, glucose, Triton X-100, Mowiol components (Mowiol, glycerol) were purchased from Sigma Aldrich (MO, USA). OCT compound (Sakura Finetek, Torrance, CA, USA). Regenerated cellulose membranes (Spectra/Por CE; Mol. Wet. Cutoff 3500) were supplied by Spectrum (Los Angeles, CA, USA). (*S*)-(–)-MRJF22 was synthetized by the research group of Prof. Agostino Marrazzo, in the Medicinal Chemistry Laboratory of the Department of Drug and Health Sciences (Università di Catania) (Barbaraci et al., 2021). All solvents (LC grade) were from VWR International (Milan, Italy).

Human corneal epithelial cell line immortalized with adenovirus 12SV40 hybrid virus (HCE-2, ATCC® CRL-11135) was purchased from LGC Standards (Barcelona, Spain), while the medium used (Keratinocyte serum-free medium added with human recombinant epidermal growth factor, bovine pituitary extract, penicillin, streptomycin, insulin) was from Thermo Fisher Scientific (Life Technologies, CA, USA).

Human uveal melanoma (UM 92-1) cell line was purchased from the Cell Factory-IST (Genova, Italy), while the medium used (RPMI-1640 medium added with fetal bovine serum (FBS), l-glutamine, penicillin and streptomycin) was from Euroclone S.p.A. (Pero, Milan, Italy).

2.2 Nanoparticles production

To produce the NLCs, the phase inversion temperature (PIT) method was chosen, following the previously described protocol (Cimino et al., 2023). Briefly, the lipid phase was composed of a mixture of surfactants (<7% w/V), the solid lipid and the liquid lipid (1:2.5 ratio). PEG 1% w/V or DDAB 0.15% w/V, were added to the lipid phase to produce pegylated nanoparticles (P-NLC) and cationic nanoparticles (D-NLC), respectively. To obtain the loaded formulations, (*S*)-(–)-MRJF22 was added at 0.02% w/V, obtaining (*S*)-NLC and
(*S*)-P-NLC. FITC at 0.01% w/V was added to obtain the fluorescent uncoated (F-NLC) and fluorescent pegylated (F-P-NLC) samples. The water and the lipid phases were heated separately and then the water phase was added dropwise in the melted oily phase under continuous stirring. The formulation was mixed at room temperature, vortexed (Heidolph Reax 2000, VWR, Milan, Italy), cooled, and then vortexed again. After 24 h, the samples were purified to remove the excess of surfactants (see section 2.3.5).

2.3 Physico-chemical and technological characterization

2.3.1 Photon Correlation Spectroscopy (PCS)

Particle size (Z-ave), polydispersity index (PDI) and zeta potential (ZP) of the samples (1:20 diluted in ultra-purified water) were measured through Photon Correlation Spectroscopy (PCS) using a ZetaSizer NanoZS (Malvern Instruments, Worcestershire, UK). Each analysis was performed at least by triplicate.

2.3.2 Osmolality and pH

An osmometer (3320 Osmometer, Advanced Instruments, Norwood, MA, USA) was used to assess the osmolality of the samples, which was previously calibrated using ultra-purified water and physiological solution. The pH values of the samples were determined using a pH meter (Mettler Toledo, Milan, Italy), calibrated using solution with defined pH 4.0, 7.0 and 10.0.

2.3.3 TEM morphology studies

Morphologies of the purified blank formulations were studied through transmission electron microscopy (TEM) using a 1:5 water dilution on a JEOL 1010 microscope (Akishima, Japan). To visualize the samples, Carbon-coated grids (carbon support film of 200 mesh from Electron Microscopy Sciences, Hatfield, United Kingdom) were used. The grids were activated using UV light, and negative staining of the samples placed on the grid was carried out using uranyl acetate (2%) (Sánchez-López et al., 2023).

2.3.4 Stability studies

To assess the physical stability of the samples, 15 mL of each unloaded sample was stored into Turbiscan® Ageing Station (TAGS, Formulaction, L'Union, France) at three different temperatures (room temperature 25.0 ± 1.0 °C, physiological temperature 36.5 ± 1.0 °C and extreme temperature 50.0 ± 1.0 °C). This technique, previously described in (Carbone et al., 2020), was selected for its well-known reliability in detecting the occurrence of aggregation and/or migration instability phenomena in colloidal suspensions (Bonaccorso et al., 2021; Carbone et al., 2014b; Puglia et al., 2020; Santonocito et al., 2020). The results were obtained as variation of transmission profiles (ΔT), which were compared between the samples, and also numerically as Turbiscan® Stability Index (TSI).

2.3.5 Encapsulation efficiency (EE%) and drug loading capacity (DLC%)

The amount of encapsulated drug was quantified indirectly as previously reported (Cimino et al., 2023). The not-entrapped drug was separated from the nanoparticles through ultracentrifugation (SL16R Centrifuge, Thermo Scientific, Rodano, Italy) at 13,000 rpm (90 min at 4 °C). The collected supernatant was diluted in methanol-0.5% diethylamine mixture (ratio 1:5) and ultracentrifuged again for 30 min. The new supernatant obtained was analyzed using UV-vis spectrophotometer (UH5300 UV-Visible Double-Beam Spectrophotometer, Hitachi Europe, Milan, Italy) to quantify the amount of (*S*)-(–)-MRJF22 at $\lambda_{222\ nm}$.

The following equation was used to calculate the encapsulation efficiency (EE%):

$$EE\% = \frac{weighted\ drug - amount\ of\ not\ entrapped\ drug}{total\ amount\ of\ drug\ used} \cdot 100$$

and the drug loading capacity (DLC%) was calculated with the equation:

$$DLC\% = \frac{amount\ of\ drug\ entrapped}{weight\ of\ lipidic\ phase} \cdot 100$$

2.4 *In vitro* studies

2.4.1 Mucoadhesion studies

Mucin suspension 0.1% w/V in simulated tear fluid, STF (NaCl 0.68 g, $NaHCO_3$ 0.22 g, $CaCl_2 \cdot 2\ H_2O$ 0.008 g, KCl 0.14 g, and distilled deionized water to 100 mL) was prepared the day before the assay and was stirred overnight. Mucoadhesive properties were analyzed by mixing mucin dispersion and nanoparticles in 1:1 V/V ratio for 15 min at 25 °C, and subsequently incubating the mixture at 37 °C, up to 4 h. Two *in vitro* methods were performed to assess the mucoadhesion at the selected time points (0, 1, 2, 3, 4 h): turbidimetric technique measuring the absorbances at $\lambda_{650\ nm}$, and mucin particle method measuring variations in Z-ave and ZP using Zetasizer Nano S90 (Malvern Instruments, Malvern, UK) (Bonaccorso et al., 2021; Cimino et al., 2023).

2.4.2 In vitro release studies

In vitro release of (*S*)-(–)-MRJF22 or FITC from nanoparticles was assessed using Franz-type diffusion cells (LGA, Berkeley, CA, USA), with 0.75 cm^2 regenerated cellulose membranes (Spectra/Por CE; Mol. Weight Cut-off 3.5 kDa) moistened for 24 h in the release medium. As reference, (*S*)-(–)-MRJF22 was solubilized in methanol-0.5% diethylamine solution (MeOH-0.5% DEA) while FITC was dissolved in ethanol (EtOH), in a concentration comparable to the encapsulated molecules into the nanosystems. Artificial tear fluid (ATF) was prepared by dissolving the salts in ultrapure water (for 1 L: $CaCl_2 \cdot 2\ H_2O$ 0.08 g, $NaHCO_3$ 2 g, NaCl 6.7 g) and adjusting the pH to 7.4 using HCl 1M, as reported in literature (Tambe et al., 2021). In the receptor, maintained at 35 ± 1 °C and stirred at 600 rpm, a 50:50 v/v mixture of tris(hydroxymethyl)aminomethane buffer (TRIS) and MeOH-0.5% DEA was used as release medium for prodrug-loaded NLCs (Cimino et al., 2023), while a 50:50 v/v mixture of ATF and EtOH supplemented with 2% w/V Tween® 80 was used to assess FITC release. The donor compartment was filled with 500 µL of each purified sample. At planned time intervals (every hour from 0 to 8 h, and then at 24 h), 500 µL were withdrawn from the receptor and replaced with medium to guarantee pseudosink conditions. Each withdrawn was diluted 1:2 with medium and analyzed using UV-vis spectrophotometer, at $\lambda_{222\ nm}$ and $\lambda_{500\ nm}$, for (*S*)-(−)-MRJF22 and FITC, respectively.

The release kinetics of the prodrug from the nanoparticles was assessed analyzing the fitting with zero order, first order, Higuchi, Hixon-Crowell and Korsmeyer-Peppas models.

2.4.3 Cell cultures

Human Corneal Epithelium HCE-2 cells were maintained in keratinocyte serum-free medium supplemented with bovine pituitary extract (BPE) 0.05 mg/mL, epidermal growth factor (EGF) 5 ng/mL, insulin 0.005 mg/mL and streptomycin 100 mg/mL. For cell viability assay, passages from 41 to 52 were used.

Human Uveal Melanoma 92-1 cells were maintained in RPMI-1640 medium, added with 10% fetal bovine serum (FBS), 2 mM L-glutamine, 100 units/mL penicillin and 100 µg/mL streptomycin. For cell viability assay, passages from 10 to 13 were used. All the cells were incubated at 37 °C and 5% CO_2.

2.4.4 Cytocompatibility

Cell viability was analyzed through 3-(4,5-dimethylthiazol-2-yl)-2,5-diphenyltetrazolium bromide (MTT) assay. The cells were seeded in 96-well plates and incubated for 48 h up to 80 % confluence. Then the medium

was removed, and the cells were treated for 5 h (for HCE-2) or 24 h (for UM 92-1) with different concentrations of NLCs, corresponding to 10 µM, 5 µM, 3 µM, 1 µM, 0.5 µM and 0.3 µM concentration of the encapsulated drug (Cimino et al., 2023). Benzalkonium chloride 0.01% was used as positive control to assess effective cell death, while medium was used as a negative, 100% viability control. After the treatment, the cells were incubated with 2.5 mg/mL MTT, then formazan crystals were solubilized in DMSO for 5 min and the absorbance was read at $\lambda_{560\ nm}$ using an automatic ModulusTM Microplate Photometer (Turner BioSystems, CA, USA) (Folle et al., 2021a, 2021b; López-Machado et al., 2021). Cell viability was expressed as the percentage of cell survival against untreated control cells.

2.4.5 In vitro ocular tolerance

HET-CAM test was used to assess *in vitro* ocular tolerance of the formulations. Chorioallantoic membrane (CAM) of 10-days embryonated eggs (provided from GALLSA farm, Tarragona, Spain) were subjected to the application of 300 µL of each sample, while NaOH 0.1N and NaCl 0.9% solutions were used as positive and negative controls, respectively (López-Machado et al., 2021). For 5 min, it was observed the appearance of hemorrhage, vasoconstriction, or coagulation. The formulations were classified as previously reported (Esteruelas et al., 2022) through the calculation of the ocular irritation index (OII) (Sánchez-López et al., 2020):

$$OII = \frac{5(301 - H)}{300} + \frac{7(301 - V)}{300} + \frac{9(301 - C)}{300}$$

Where H, V and C are the time of appearance of hemorrhage, vasoconstriction and coagulation, respectively, expressed in seconds. Results were classified as: not-irritant ($0 < OII < 0.9$), slightly irritant ($1 < OII < 4.0$), moderately irritant ($5 < OII < 8.9$), or severely irritant ($9 < OII < 21$).

Moreover, a quantitative irritation measurement was carried out through the HET-CAM TBS assay. 1000 µL of 0.1% trypan blue staining (TBS) in phosphate buffered saline (pH 7.4) solution were added to the previously treated CAM for 1 min and then washed with distilled water to remove the excess of TBS. The CAM was then excised and weighted, then was put into 5 mL of formamide to extract the absorbed TBS, which was quantified through NanoDrop™ (One/One^C Microvolume UV-Vis Spectrophotometer, Thermo Fisher Scientific, Waltham, Massachusetts, USA) at $\lambda_{595\ nm}$. The quantification of the absorbed dye (AD) was calculated using the following equation:

$$AD = \frac{absorbance}{membrane\ weight\ (mg)} \cdot \frac{5}{1000} \cdot\ 10^9\ nmol$$

Considering the obtained values, the samples were classified using the following scale: ≤ 0.19 nmol/mg not irritant; 0.10-0.15 nmol/mg moderately irritant; ≥ 0.15 nmol/mg severely irritant (Esteruelas et al., 2022).

2.5 *In vivo* studies

2.5.1 Draize irritation test

Draize irritation test (Sánchez-López et al., 2016) was performed on 2 kg New Zealand albino rabbits purchased from Granja Riera and housed in individual cages. Animals were maintained in controlled temperature (17-23 °C) and relative humidity (60-80% RH) conditions, with food and water supplemented *ad libitum*. This test was carried out in accordance with the Ethical Committee for Animal Experimentation of the University of Barcelona and current legislation (Decree 214/97, Gencat).

In order to perform the assessment, 50 µL of the loaded NLCs and of (*S*)-(–)-MRJF22 solution were administered topically in the conjunctival sac, performing a light massage to distribute the sample on the entire surface of the eye. After 30 min, cornea, conjunctiva and iris were observed to highlight eventual damages, following the guidelines reported in Supplementary Table 1 and using the equation below to calculate the ocular irritation index (OII).

$$OII = Corneal(A \cdot B \cdot 5) + Iris(A \cdot 5) + Conjunctiva(A + B + C) \cdot 2$$

The obtained scores were classified as follow: 0 non-irritant, 0-15 slightly irritant, ≥ 15-30 moderately irritant, ≥ 30-50 irritant, ≥ 50 severely irritant (Esteruelas et al., 2022).

2.5.2 Antiangiogenic capacity

Antiangiogenic capacity of the samples was assessed using the CAM assay (Esteruelas et al., 2022). To perform the analysis, a window in the shell was opened on the side of 3 days fertilized eggs, and, after 24 h of incubation at 37 °C and 85% humidity, the CAM was treated with 40 µL of each sample. After 48 h of treatment, the CAM was fixed with 4% paraformaldehyde at 4 °C. After 24 h, membranes were removed and observed through binocular loupe. The density of the vessels was measured automatically using ImageJ vessel analysis plugin (Sánchez-López et al., 2023).

2.5.3 Ocular anti-inflammatory prevention

In vivo preventive anti-inflammatory activity was analyzed on New Zealand albino rabbits. Samples were administered and after 30 min an inflammatory stimulus was applied by adding sodium arachidonate 0.5% w/V. The occurrence of ocular damage was assessed after 30 min and then at 1, 1.5, 2, 2.5 h (Vega et al., 2006). Ocular irritation index was evaluated based on the criteria described in Supplementary Table 1 (Esteruelas et al., 2022) and using the equation reported in section 2.5.1.

2.5.4 In vivo biodistribution images

In vivo biodistribution images were obtained by applying two 50 µL-administrations separated by 5 min of clearance of either fluorescent-NLCs or FITC solution into the conjunctival sac of New Zealand albino rabbits, massaging the eye after each administration. After 3 h, the animals were sacrificed and the eyes were enucleated and transferred into paraformaldehyde 4% in PBS, and then frozen at -80 °C.

Afterwards, the frozen eyes were cut using a cryostat (Leica CM 3050 S, Leica Microsystems GmbH, Wetzlar, Germany) and the cellular nucleus were stained with DAPI. Fluorescence images were obtained using a Leica Thunder Imager DMI8 (Leica Microsystems GmbH, Wetzlar, Germany), with a 5x objective, and quantified using ImageJ software (Swetledge et al., 2021).

2.6 Statistics

For the characterization of blank, loaded and fluorescent formulations, ordinary one-way ANOVA with Tukey's multiple comparison test was used: blank P-NLC and D-NLC were compared to NLC, while the loaded and the fluorescent samples were compared to their respective blanks. For mucoadhesive studies, two-way ANOVA was performed, using Tukey's multiple comparisons test for mucin particle method and

Dunnett's multiple comparisons test for the turbidimetric assay. For cytocompatibility, two-way ANOVA with Dunnett's multiple comparisons test was performed compared to CTRL, as well as for HET-CAM, HET-CAM TBS, *in vitro* antiangiogenic capability assay and *in vivo* anti-inflammatory activity test. All analyses were performed with GraphPad Prism 9.5.0 (GraphPad Software, Inc., San Diego, CA) and p values were considered significant at $p \leq 0.05$.

3. Results and discussion

3.1 Physico-chemical and technological characterization of unloaded NLCs

As already described in a previous work (Cimino et al., 2023), the PIT method – which is a green and organic solvent-free preparation technique – and the raw materials were selected for their capability to allow the formation of NLCs with small and homogeneous mean diameters. Moreover, all the materials demonstrated to be well-tolerated for ocular topical administration, as already discussed elsewhere (Bonaccorso et al., 2021). A blank nanosystem was prepared (NLC) and compared to surface-modified P-NLC and D-NLC, respectively obtained with the addition of PEG or the cationic lipid DDAB. In fact, in literature it was extensively demonstrated that enhanced nanoparticle permeation (Razavi et al., 2022) could be obtained through cationic surface modification of the nanoparticles because of the higher mucoadhesiveness on ocular surface (Bonaccorso et al., 2021; Niamprem et al., 2019) through ionic interaction with mucin (Bonaccorso et al., 2021; Nirbhavane et al., 2020). On the other hand, PEGylation mainly increases the retention time on corneal surface due to the ability of interpenetrate the mucin chains (Grassiri et al., 2021) thus allowing a prolonged release (Niamprem et al., 2019; Razavi et al., 2022).

As reported in Figure 1, Zetasizer analysis confirmed the homogeneity of the samples, with PDI values lower than 0.25 and a mean particles size lower than 160 nm, without significant variations among them. The slight not significant increase in Z-ave reported for P-NLC may be related to the presence of the PEG coating, as demonstrated by Jokerst (Jokerst et al., 2011), while the slight not significant decrease in the mean diameter of D-NLC may be caused by the addition of DDAB which was previously demonstrated to reduce particle size when compared to uncoated formulation (Date et al., 2011). It is well-known that Z-ave is a crucial parameter for the ophthalmic administration, since particle diameters higher than 10 μm are not well-tolerated, and in particular a mean particle size between 50 and 400 nm is preferred to avoid ocular irritation (Silva et al., 2021). Furthermore, particle size strongly influences the distribution and the residence time of the carriers in the various ocular structures (Bonaccorso et al., 2021), where diameters lower than 200 nm are mandatory to allow ocular permeation (Onugwu et al., 2022) and to enhance mucoadhesion and endocytosis (Niamprem et al., 2019). The slight increase in the PDI value of P-NLC, in comparison with NLC and D-NLC, is however not statistically significant, and all the samples are considered homogeneous (values lower than 0.3). Moreover, the ZP of the samples was measured (data can be found in Supplementary Table 2), since it allows to predict the long-term stability of the samples, basing on the idea that markedly positive or negative values could guarantee particle repulsion thus avoiding physical instability phenomena (Musumeci et al., 2019). The obtained results showed neutral ZP values for NLC and P-NLC, while D-NLC resulted positively charged (+24.9 ± 0.67 mV), as expected.

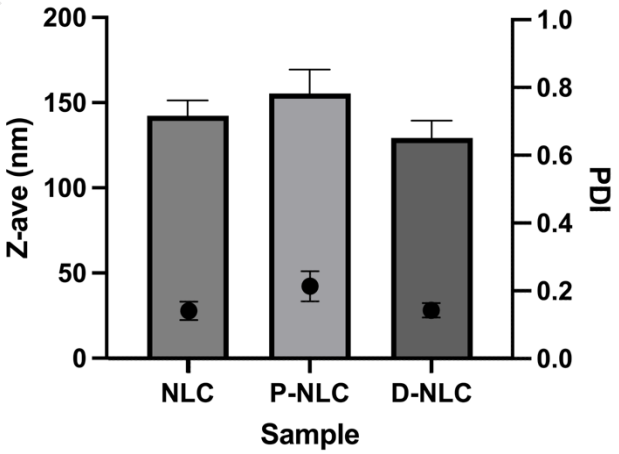

Figure 1. Z-ave (nm) and PDI values of NLC, P-NLC, and D-NLC. Values are reported as mean of at least 3 measurements ± SD. Not significant for $p \leq 0.05$.

The prepared formulations were adjusted to accomplish other requirements of both European Pharmacopoeia and FDA for ocular formulations, namely pH and osmolality (data can be found on Supplementary Table 2), which should fall between the range tolerated by the eye. In particular, pH should be between 6.8 and 7.4 (Pignatello, 2014) to avoid ocular chemical damage (Lim et al., 2014), while osmolality should be in the tear range (280 and 300 mOsm/kg) to allow a safe passage of particles through the biological membranes (Bonaccorso et al., 2021).

TEM images reported in Figure 2 confirmed small mean particle diameters for all the formulations, lower than 200 nm, with NLC and D-NLC showing a greater homogeneity compared to P-NLC, in accordance with PDI values (Figure 1). The shape of the particles resulted to be spherical, and no morphological changes were highlighted after the addition of the DDAB or PEG coatings (Carbone et al., 2014a), (Karmakar et al., 2018).

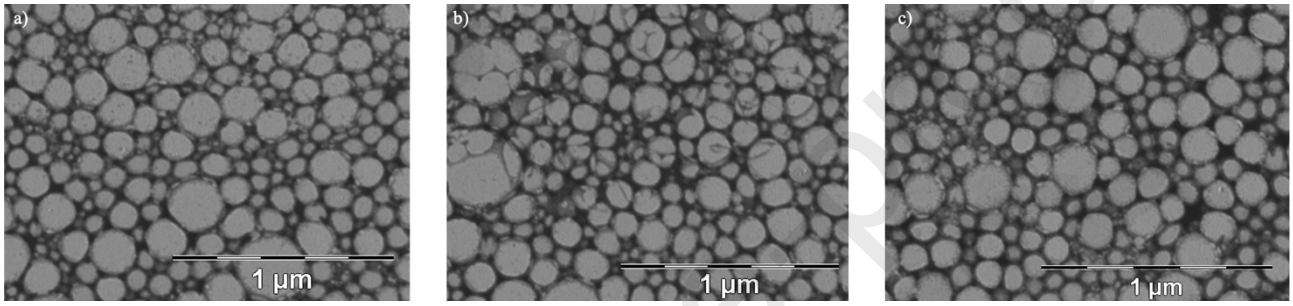

Figure 2. TEM images of NLC (**a**); D-NLC (**b**); P-NLC (**c**).

The stability of the samples was verified using the Turbiscan® Technology equipped with an Ageing Station. The variation of transmission profiles (ΔT) is a parameter which describes physical instability in the sample, discerning if it is occurring a particle size increment, identified as higher ΔT values in the middle of the graph, or a particle migration phenomenon, when ΔT increasing are located in the lateral parts of the graph, depending on the type of instability phenomenon occurring (clarification, sedimentation or creaming) (Carbone et al., 2014a). As reported in Figure 3, a not significant variation of transmission ($\Delta T << 10\%$) was observed at the bottom of the cuvette in all the samples stored at 25 °C, related to the formation of a slight sediment which was easily redispersed by gentle shaking of the colloidal suspension. The same behavior was observed at 36.5 °C and 50 °C (data not showed). The destabilization kinetics, shown in Supplementary Figure 1 in terms of evolution of Turbiscan® Stability Index (TSI), demonstrated a high stability of all the samples at all the analyzed temperatures. The slightly higher stability of D-NLC reflects its higher ZP value, which guarantee particle repulsion thus stability, as already discussed, and confirms previous literature findings (Carbone et al., 2014a).

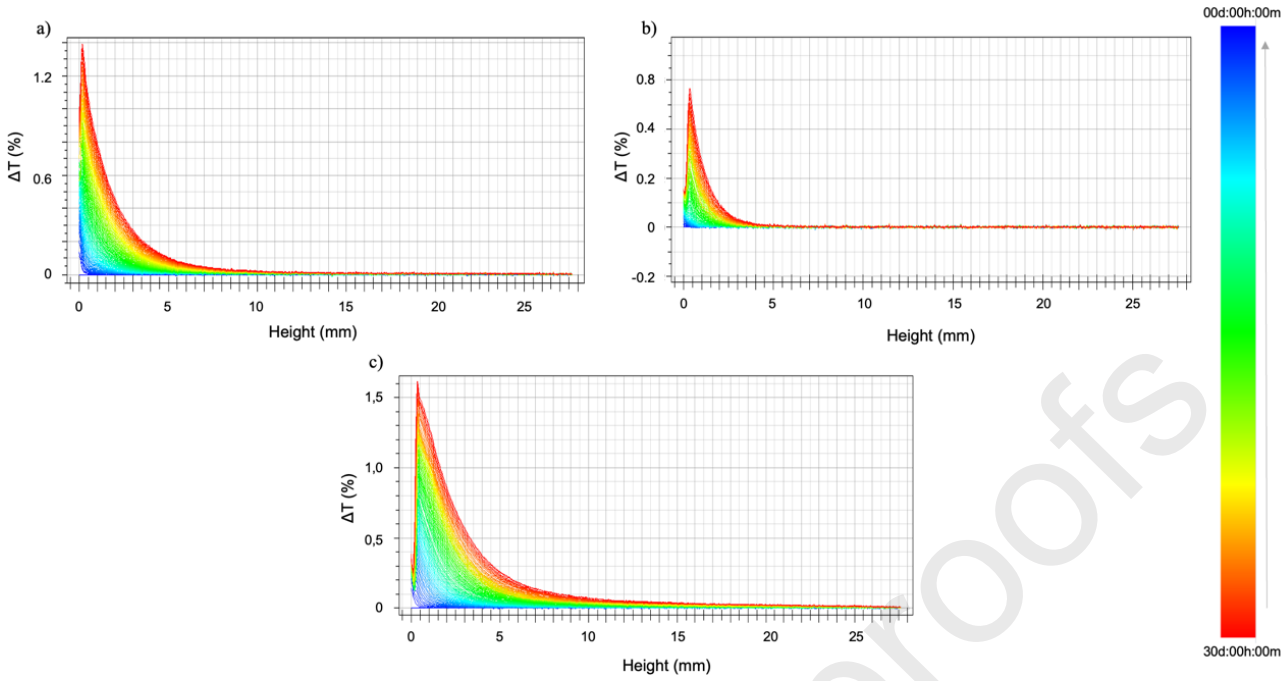

Figure 3. Variations of transmission (ΔT) profiles of samples NLC (**a**), D-NLC (**b**) and P-NLC (**c**) after 30 days of storage in Turbiscan® at 25.0 ± 1.0 °C, data are represented as a function of time (0-30 days) of sample height (0-25 mm) – the sense of analysis time is indicated by the arrow.

3.2 *In vitro* studies on unloaded NLCs

3.2.1 In vitro cytocompatibility

The HCE-2 (human corneal epithelium) cell line was selected to analyze the compatibility of the formulations on corneal cells after topical administration. Samples were added to the cells and further incubated for 5 h, since the physiological clearance mechanisms of the eye usually do not allow a longer residence time (Kiss et al., 2020). Considering that the NLCs were developed for the delivery of (*S*)-(–)-MRJF22 for the potential treatment of UM, cytocompatibility studies were also performed on UM 92-1 (uveal melanoma) cell line. NLCs dilutions were selected in order to encapsulate an amount of prodrug comparable to its therapeutic dose (Barbaraci et al., 2021), and consistently with previous results obtained in the dose-response curves on fibroblasts (Carbone et al., 2020) and uveal melanoma cells (Cimino et al., 2023).

As a positive cytotoxic control, BAK 0.01% was also applied (Bonaccorso et al., 2021). In cells treated with BAK, cell viability values were 6.64% for HCE-2 cells and 4.21% for UM 92-1 cells. Blank NLC (Figure 4 a,d) and P-NLC (Figure 4 b,e) showed a dose-depended effect on the viability of both cell lines, with NLC being safe (viability > 80%) up to 1 µM, and P-NLC until 3 µM. On the opposite, D-NLC showed high cytotoxicity on both cell lines (Figure 4 c,f), with a drastic decrease in the viability even at the lowest concentrations tested. This behavior is probably related to the presence of the cationic DDAB, whose ability to electrostatically interact with the anionic ocular surface could affect the cell viability (Razavi et al., 2022). For its cytotoxicity, D-NLC was not subjected to further studies.

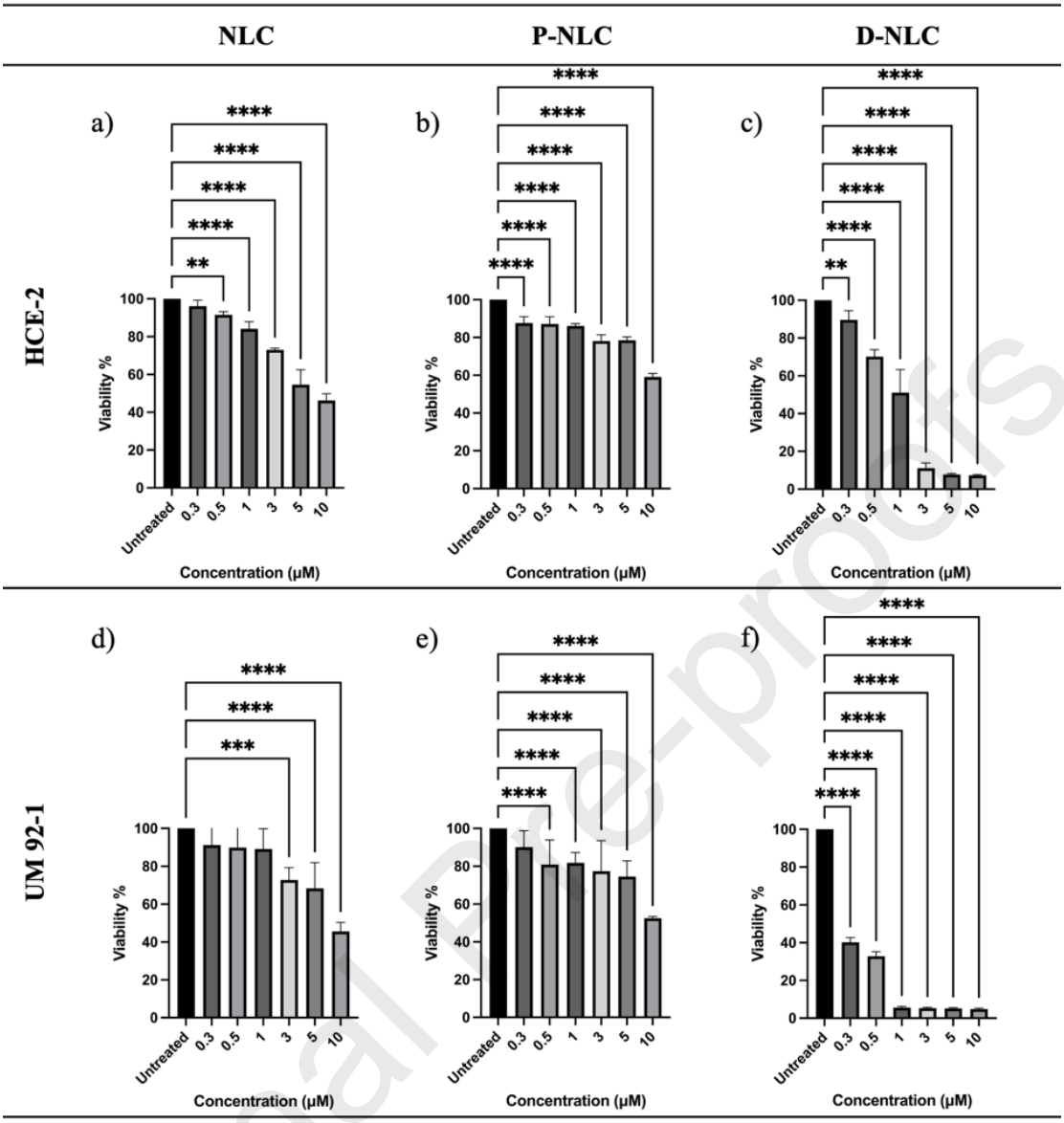

Figure 4. Cytocompatibility on HCE-2 cells (**a-c**) and on UM 92-1 cells (**d-f**) of: NLC (**a,d**); P-NLC (**b,e**); D-NLC (**c,f**). Values are reported as mean of at least 3 independent experiments ± SD. Significance was set at ** $p \leq 0.01$; *** $p \leq 0.001$; **** $p \leq 0.0001$.

3.2.2 In vitro mucoadhesion properties

To further assess the interaction of the nanoparticles with the ocular surface, *in vitro* mucoadhesion studies were performed on uncoated NLC and PEGylated P-NLC; in fact, after ophthalmic administration, the nanoparticles need to interact with ocular surface – which contains mucin, a high-molecular weight glycoprotein characterized by a negative ZP – in order to avoid the elimination with the tears. This interaction should not be excessively strong, thus to achieve the posterior segment without remaining adhered on the ocular surface.

Mucoadhesive properties of the nanoparticles was firstly assessed by mucin particle method, in which interaction with mucin is measured analyzing the changes in Z-ave and ZP values. As reported in Figure 5 a, both the samples demonstrated to slightly interact with mucin, as highlighted by the significant increase (**** $p \leq 0.0001$) in particle size of muc-NLC and muc-P-NLC compared to NLC and P-NLC at all analyzed timepoints. ZP measurements confirmed these interactions, as a significant reduction (*** $p \leq 0.001$,

**** $p \leq 0.0001$) in ZP values of the samples after incubation with mucin was reported at all timepoints (Figure 5 b). The occurrence of mild interaction was also highlighted by the slight increase of PDI values for both samples, from 0.18 to 0.38 for NLC, and from 0.23 to 0.35 for P-NLC (however results were not significant). These results were confirmed also by the turbidimetric assay (Figure 5 c), which estimates the mucoadhesiveness basing on the assumption that the interaction of the nanoparticle with mucin causes an aggregation that could be detected by UV-vis analysis. As previously reported, PEG did not increase mucoadhesiveness compared to the uncoated NLC (Bonaccorso et al., 2018). The interactions with mucin suggest that both systems could be retained on the ocular surface, avoiding the loss related to the tears flow. However, it resulted necessary to assess their capability to migrate to the posterior chamber and to not remain indefinitely adhered on the ocular surface, as successively preliminary investigated through *in vivo* biodistribution images.

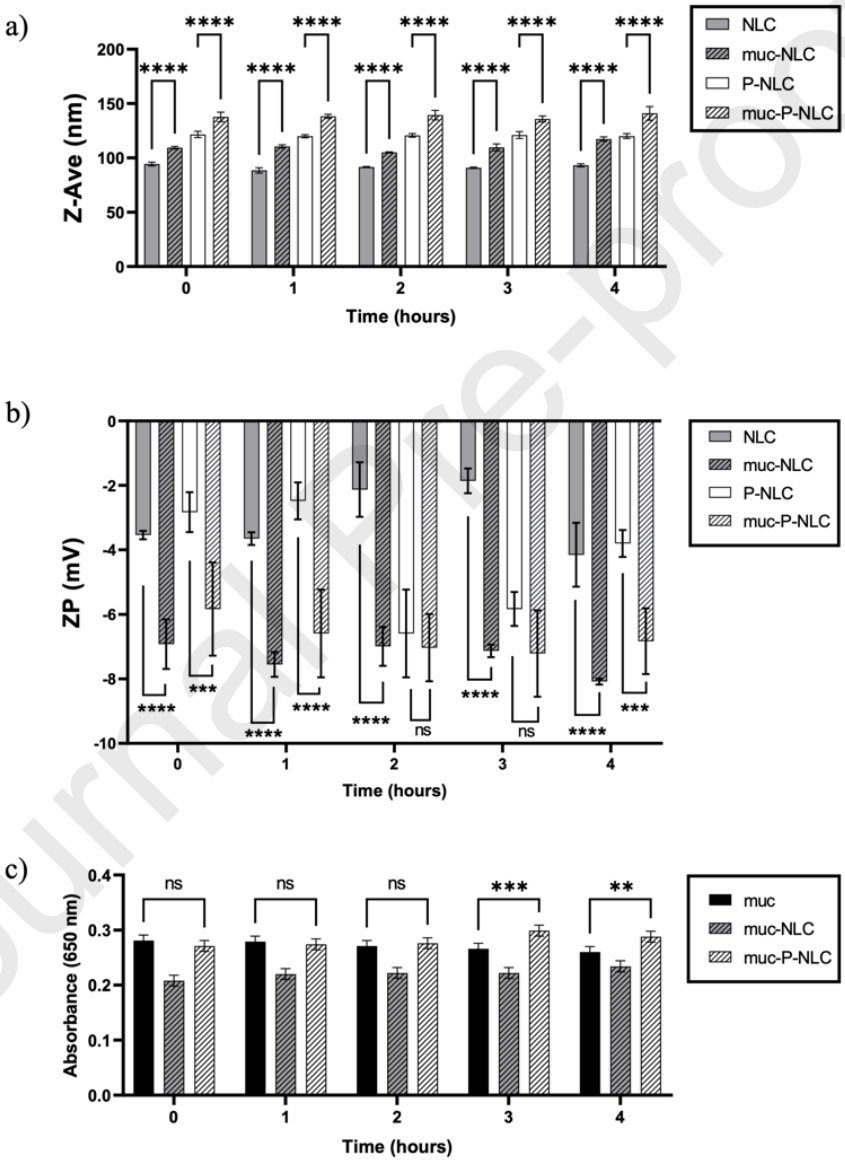

Figure 5. Z-ave values (**a**) and ZP values (**b**) of samples (NLC and P-NLC) before 0 and after 1, 2, 3 and 4 h of incubation with mucin (muc-NLC, muc-P-NLC) at 37 °C. Significance was set at *** $p \leq 0.001$; **** $p \leq 0.0001$. (**c**) *In vitro* assessment of samples/mucin interactions at different time points (0, 1, 2, 3 and 4 h) by turbidimetric assay at $\lambda_{650\ nm}$. Significance was set at ** $p \leq 0.01$; *** $p \leq 0.001$. Values are reported as mean of at least 3 measurements ± SD.

3.3 Physico-chemical and technological characterization of loaded NLCs

Since NLC and P-NLC were developed to possess interesting features for potential ophthalmic administration, both colloidal systems were loaded with (*S*)-(–)-MRJF22, a new prodrug synthetized combining valproic acid (VPA) and haloperidol metabolite II (HP-II) (Barbaraci et al., 2021). Basing on our previous findings (Cimino et al., 2023), (*S*)-(–)-MRJF22 was added to the nanoparticle's composition at 0.02% w/w, obtaining (*S*)-NLC and (*S*)-P-NLC, with an encapsulation efficiency of 57.73 ± 1.91% and of 52.89 ± 2.90% respectively, thus in line with previous results obtained for the same prodrug delivered into a similar NLC platform (Cimino et al., 2023). Drug loading capacity was also measured, resulting to be 0.083 ± 0.001% and 0.073 ± 0.002% for (*S*)-NLC and (*S*)-P-NLC, respectively. The Zetasizer characterization of both the loaded samples confirmed that the Z-ave, PDI and ZP values were not significantly altered by the encapsulation of the prodrug, as well as the physiological pH and osmolality values (Supplementary Table 2).

Release profiles of (*S*)-(–)-MRJF22 from uncoated NLC and PEGylated P-NLC were analyzed using Franz type diffusion cells (Figure 6): a similar behavior characterized by a slow and prolonged release was observed for both the formulations. This behavior, which is extensively reported in literature for NLCs (Balguri et al., 2016; Ortiz et al., 2021), is usually attributable to the diffusion of the drug from the lipid matrix (Balguri et al., 2016). The initial release at the beginning of the experiment (9.89% for S-NLC) and 9.07% for P-NLC) suggests that there is a drug-rich region localized on the surfactant layer of the nanoparticles (Makoni et al., 2019). After 8 h, (*S*)-NLC and (*S*)-P-NLC released 14.00% and 16.47% of the encapsulated (*S*)-(–)-MRJF22 respectively, to reach then 28.20% and 19.78% of prodrug released (from (*S*)-NLC and (*S*)-P-NLC respectively) after 24 h of treatment, resulting in line with previous findings (Cimino et al., 2023). The difference between the two samples at 24 h is probably related to the presence of PEG coating, which is known to provide a sustained and slow release (Duncan et al., 2019). The two release profiles were correlated with different models (zero order, first order, Higuchi, Hixon-Crowell and Korsmeyer-Peppas). The uncoated (*S*)-NLC showed a best fit with zero order model (R^2 = 0.98), which is very common for NLC platforms. On the other hand, PEGylated (*S*)-P-NLC showed a best fit with Higuchi model (R^2 = 0.919), typical of drug enriched shell lipid nanoparticles (Liu et al., 2020), but a great correlation was found also with Korsmeyer-Peppas model (R^2 = 0.913), which is characteristic for lipid nanoparticles (Liu et al., 2020). The obtained release profiles were compared with (*S*)-(–)-MRJF22 solution, which showed an initial release of 44.48% at the very beginning of the experiment, to reach a complete release after 3 h. This confirms the importance of the encapsulation into drug delivery systems to provide a prolonged and sustained release of the active molecule, compared to the drug solution (Balguri et al., 2016).

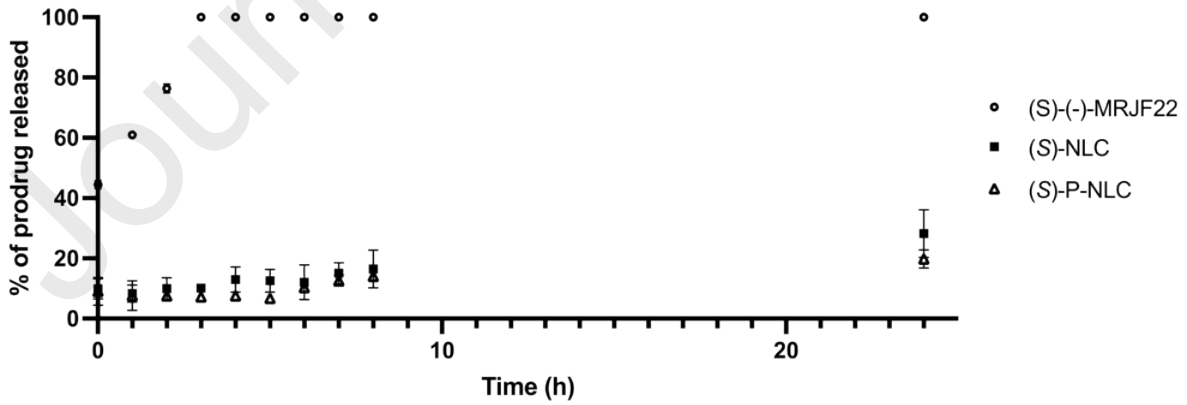

Figure 6. Release profiles of (*S*)-(–)-MRJF22 from (*S*)-NLC and (*S*)-P-NLC, compared to (*S*)-(–)-MRJF22 solution.

3.4 *In vitro* studies on loaded NLCs

3.4.1 In vitro cytocompatibility

The cytocompatibility of (*S*)-(–)-MRJF22 solution and of the loaded samples was evaluated as previously reported for the blank formulations (Figure 4 a,d).

A certain toxicity was observed for the prodrug solution on corneal HCE-2 cells, being safe only at concentrations lower that 1 μM (viability = 80.54%). It was interesting to note that the encapsulation into NLCs greatly improved the prodrug cytocompatibility up on HCE-2 cells to 5 μM for (*S*)-NLC (viability = 78.97%) and (*S*)-P-NLC (viability = 74.47%). In tumoral UM 92-1 cells, the same 5 μM concentration resulted in a viability of 62.71%, 65.87% and 59.18%, for (*S*)-(–)-MRJF22, (*S*)-NLC and (*S*)-P-NLC, respectively. Considering that previous studies demonstrated that (*S*)-(–)-MRJF22 has antiproliferative efficacy for UM treatment at concentrations ≥ 5 μM (Barbaraci et al., 2021), the encapsulation of the prodrug into both NLC and P-NLC demonstrated to protect the HCE-2 cell from the potential corneal toxicity of the prodrug, while maintaining unaltered its effect on the target UM 92-1 cells, highlighting the potentiality of the nanocarriers in the treatment of uveal melanoma.

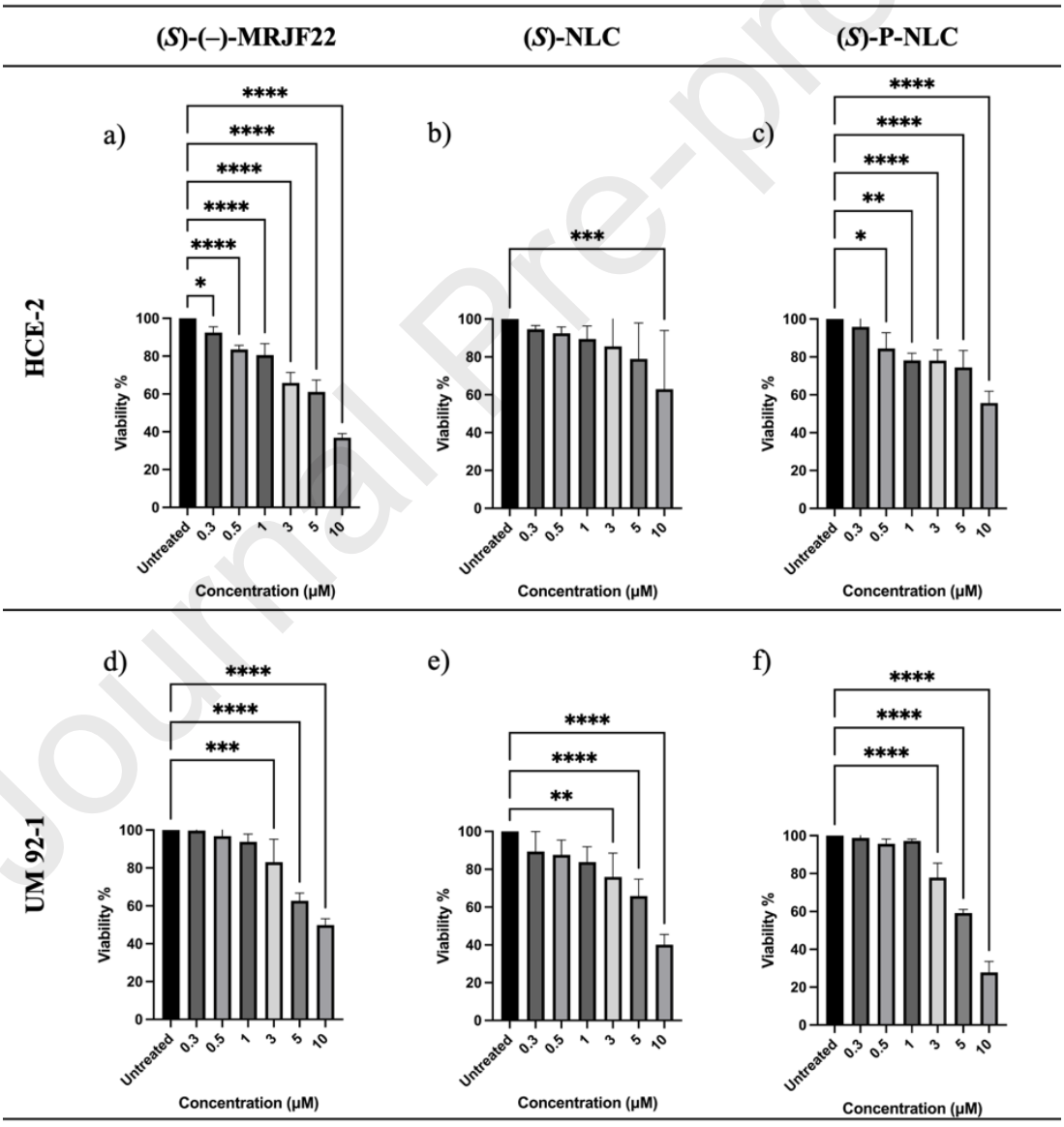

Figure 7. Cytocompatibility on HCE-2 cells (**a-c**) and on UM 92-1 cells (**d-f**) of: (*S*)-(–)-MRJF22 (**a,d**); (*S*)-NLC (**b,e**); (*S*)-P-NLC (**c,f**). Values are reported as mean of at least 3 independent experiments ± SD. Significance was set at * $p \leq 0.05$; ** $p \leq 0.01$; *** $p \leq 0.001$; **** $p \leq 0.0001$.

3.4.2 In vitro ocular tolerance

In order to confirm the *in vitro* ocular tolerance of the samples, the HET-CAM test was performed, which is based on the analysis of the vascular damage on the blood vessels of the CAM (Anantaworasakul et al., 2020), which are comparable to the ones of the rabbit conjunctiva. Subsequently, also the HET-CAM TBS was developed as a quantitative assay (Oliveira et al., 2012). From the HET-CAM results (Figure 8 a-b) it clearly emerged that both (*S*)-NLC and (*S*)-P-NLC were safe and did not show any irritant effect, while for (*S*)-(–)-MRJF22 solution all the three reported events (vasoconstriction, hemorrhage, and coagulation) were recorded, with values falling in the moderate irritation range. An additional assessment was carried out by means of the HET-CAM TBS test (Figure 8 c), which actually confirmed the non-irritant properties of both nanosystems (OII ≤ 0.9, AD ≤ 0.10 nmol/mg) (Esteruelas et al., 2022) and the moderately irritant behavior of (*S*)-(–)-MRJF22 (OII = 5-8.9; AD = 0.10-0.15 nmol/mg). These results are in agreement with the cytocompatibility on HCE-2 corneal cells, which highlighted an increase of (*S*)-(–)-MRJF22 biocompatibility when encapsulated into the nanosystems, compared to the free prodrug, and with previous literature findings on the safety of NLC systems (Aher et al., 2021; Varela-Fernández et al., 2022).

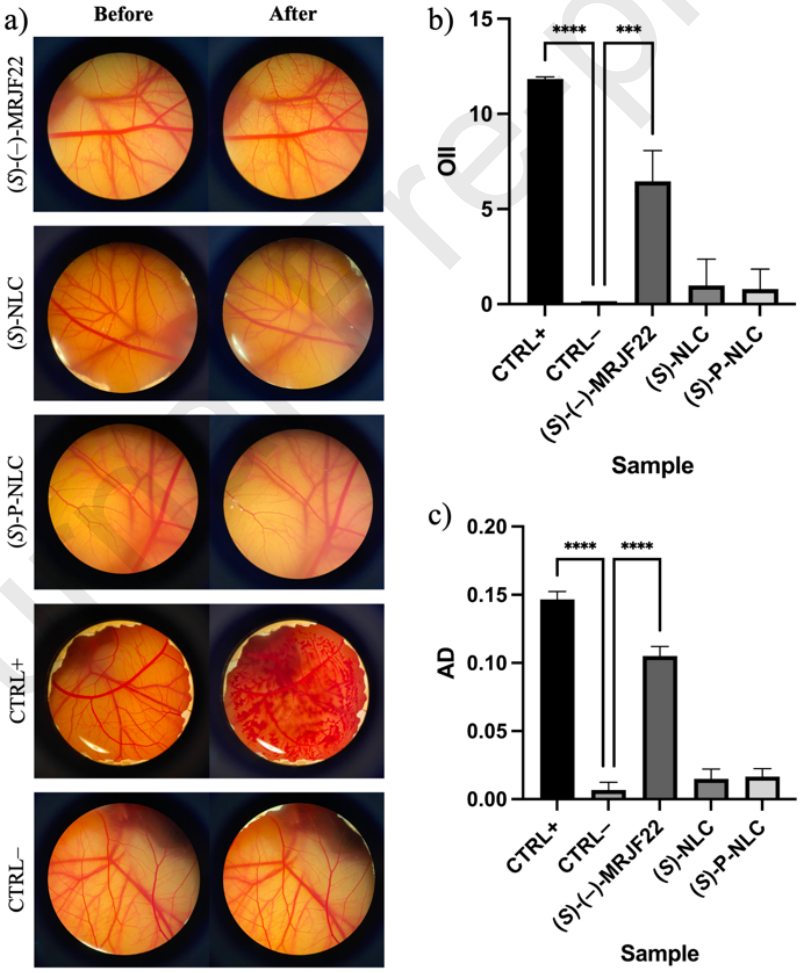

Figure 8. (**a**) HET-CAM images, before and after the treatment with (from the top): (*S*)-(–)-MRJF22 solution, (*S*)-NLC, (*S*)-P-NLC, CTRL+ (NaOH) and CTRL– (NaCl). (**b**) Ocular irritation index (OII) results from HET-CAM test. (**c**) Absorbed dye (AD) values (nmols/mg) from HET-CAM TBS assay. Significance was set at *** $p \leq 0.001$; **** $p \leq 0.0001$ compared to CTRL–.

3.5 *In vivo* studies on loaded NLCs

3.5.1 Draize irritation test

As a further confirmation of the ocular tolerance of the samples, *in vivo* Draize test was performed on New Zealand albino rabbits (Adibkia et al., 2007). Both (*S*)-NLC and (*S*)-P-NLC and the (*S*)-(–)-MRJF22 solution were topically administered, and, after 30 min, corneas were examined and the results obtained (Figure 9 a-b) confirmed that the free (*S*)-(–)-MRJF22 solution caused an irritation phenomenon, while both the loaded formulations produced ocular irritation indexes significantly lower than the positive control ($^{**}p \leq 0.01$; $p \leq 0.001$ for (*S*)-NLC and (*S*)-P-NLC, respectively). These results, together with those obtained from cytocompatibility test on HCE-2 cells and from HET-CAM test, confirm the nanoencapsulation represents a successful strategy to improve prodrug tolerability on ocular tissues, reducing the potential ocular irritative side effect of the loaded prodrug.

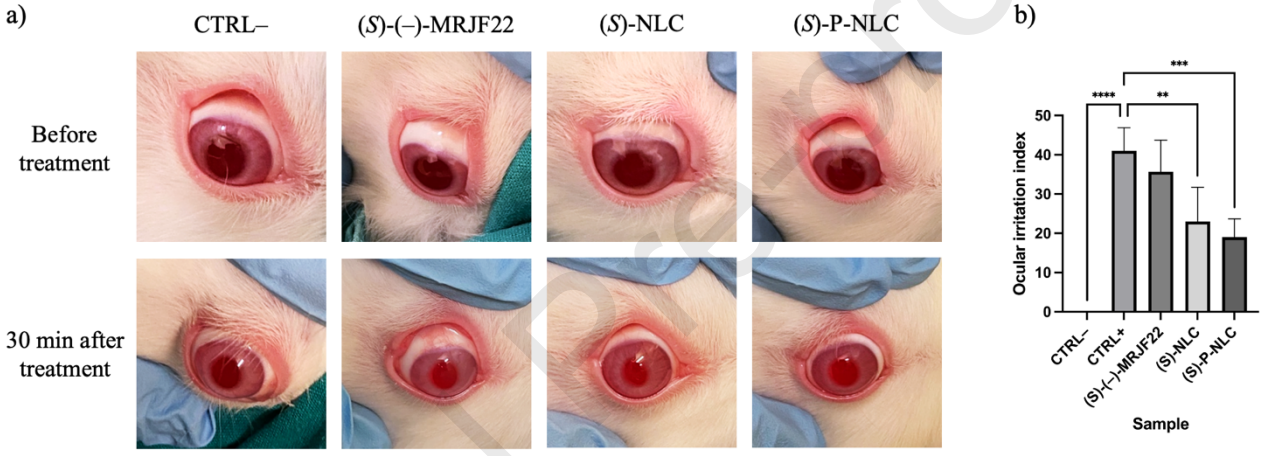

Figure 9. *In vivo* ocular tolerance Draize test: (**a**) images before and after 30 min of treatment with (*S*)-(–)-MRJF22 solution, (*S*)-NLC and (*S*)-P-NLC on New Zealand albino rabbits; (**b**) ocular irritation indexes after 30 min of treatment. Significance of ocular irritation index was set at $^{**}p \leq 0.01$; $^{***}p \leq 0.001$; $^{****}p \leq 0.0001$ compared to CTRL+.

3.5.2 Antiangiogenic capacity

The activity of (*S*)-(–)-MRJF22 on VEGF-A was previously assessed on HREC cells through the tube formation assay, both in presence and absence of VEGF-A, demonstrating the applicability of the prodrug in the regulation of σ receptor pathways, thus acting in cell migration of UM. Basing on these considerations, the present antiangiogenic capacity test was aimed to the comparison between the activity of the prodrug-loaded formulation and the free prodrug solution. The antiangiogenic activity of (*S*)-NLC, (*S*)-P-NLC and (*S*)-(–)-MRJF22 solution was analyzed *in vivo* measuring the vessel density % on CAM membranes after 48 h of treatment (Sánchez-López et al., 2023). As can be observed in Figure 10 a, all the tested samples produced an important antiangiogenic effect, with a significant decrease ($^{****}p \leq 0.0001$) in vessel density % compared to both NaCl negative control and bFGF positive control (bFGF significance was $^{****}p \leq 0.0001$ for (*S*)-NLC, (*S*)-P-NLC and (*S*)-(–)-MRJF22 solution). No significant difference was observed between the uncoated and the PEGylated NLC in respect to the free prodrug. This result confirms that the loading of the prodrug in NLC and P-NLC did not affect its therapeutic efficacy. In fact, previous studies carried on (*S*)-(–)-MRJF22 (Barbaraci et al., 2021) demonstrated the capability of this prodrug to counteract the pro-angiogenic action of VEGF-A. In detail, the σ_2 binding affinity of (*S*)-(–)-MRJF22 was demonstrated to be able to inhibit VEGF-A, which

mediates cell proliferation, tube formation and, more importantly, cell motility, that is responsible of the high metastatic progression of UM (Seftor et al., 2002).

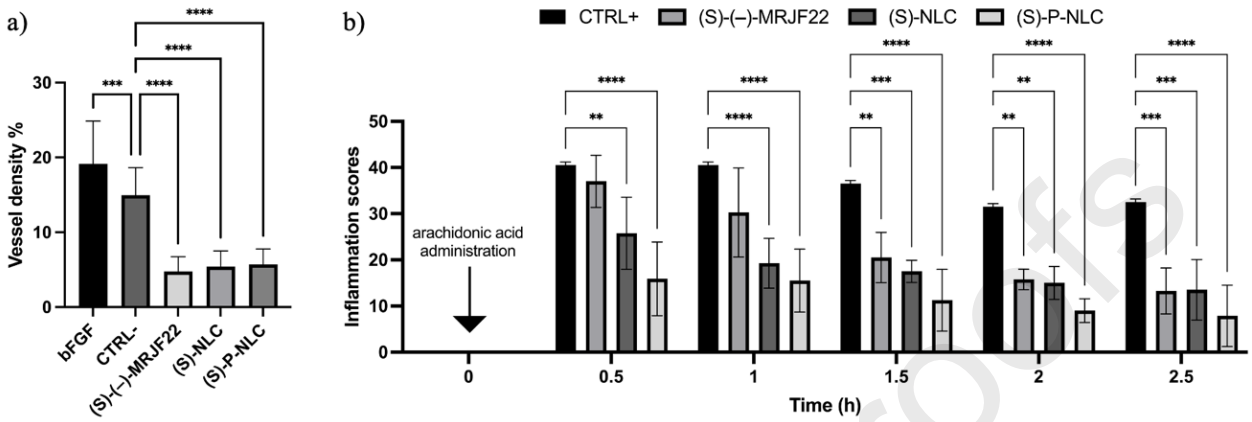

Figure 10. (**a**) Antiangiogenic activity of (*S*)-(–)-MRJF22 solution, (*S*)-NLC and (*S*)-P-NLC on 3 days fertilized eggs, after 48 h of treatment, compared to bFGF (CTRL+) and NaCl (CTRL–). Significance was set at *** $p \leq 0.001$; **** $p \leq 0.0001$ compared to CTRL–. (**b**) *In vivo* prevention of inflammation test performed on New Zealand albino rabbits treated 30 min with NaCl (CTRL+), (*S*)-(–)-MRJF22 solution, (*S*)-NLC and (*S*)-P-NLC, inflamed with arachidonic acid and analyzed at different timepoints. Significance was set at * $p \leq 0.05$; ** $p \leq 0.01$; *** $p \leq 0.001$; **** $p \leq 0.0001$ compared to CTRL+.

3.5.3 Ocular anti-inflammatory capacity

Since UM is characterized by an inflammatory phenotype (Bronkhorst and Jager, 2013) which involves immune cells as T lymphocytes (De Waard-Siebinga et al., 1996), the capability of the samples to prevent ocular inflammation was assessed *in vivo* on New Zealand albino rabbits (Esteruelas et al., 2022; Vega et al., 2006). As highlighted in Figure 10 b, (*S*)-(–)-MRJF22 solution caused an initial slight decrease of the inflammation compared to control, followed by a progressive improvement of this activity, demonstrating that the prodrug possesses a protective capacity against inflammation. This protective activity was enhanced by the encapsulation of (*S*)-(–)-MRJF22 into nanoparticles, since, after 30 min from the inflammatory stimulus, (*S*)-NLC and (*S*)-P-NLC were able to provide a 1.5-fold and 2.5-fold reduction (significance: **** $p \leq 0.0001$) compared to the free prodrug solution, respectively. At the end of the experiment all the formulations demonstrated to be able to provide a significant anti-inflammatory activity. The improvement of (*S*)-(–)-MRJF22 anti-inflammatory activity when encapsulated into the carriers could be related to the ability to protect the cornea from the irritant action of the free prodrug, as demonstrated by Draize test, and also to the slight mucoadhesive properties of the nanoparticles, which guarantee an adequate residence time on ocular surface allowing a prolonged release of the drug. Furthermore, the higher anti-inflammatory activity of (*S*)-P-NLC compared to (*S*)-NLC could be attributable to the presence of PEG 1500, which already demonstrated to have anti-inflammatory properties itself (Aghaie et al., 2019).

3.5.4 Fluorescent NLCs and preliminary in vivo biodistribution images

Aiming to visualize the distribution of the NLCs after topical ophthalmic administration, FITC was selected as lipophilic probe, since the use of fluorescein in ocular biodistribution studies is reported in literature (Jounaki et al., 2021; Kakkar et al., 2021; Shen et al., 2010), as well as for its established use in ophthalmic diagnostic practice. The addition of the fluorescent probe did not modified nanoparticles feature in terms of mean size, homogeneity and ZP (data not reported). Release profiles of FITC from F-NLC and F-P-NLC, compared to FITC solution, are reported in Supplementary Figure 2.

Considering the comparable results obtained from the mucoadhesion experiments, as well as the higher anti-inflammatory activity reported in the lasts analyzed timepoints, 3 h was selected as the biodistribution time. In line with literature findings (Jounaki et al., 2021), FITC demonstrated to be suitable for biodistribution studies since at 3 h it provided a 35.43% release from the probe solution and a < 10% release from both F-NLC and F-P-NLC.

F-NLC, F-P-NLC and FITC solution were topically administered on New Zealand albino rabbits, to visualize the *in vivo* biodistribution of the samples through fluorescence microscopy analysis. The obtained fluorescence images, reported in Figure 11 a-b, suggested that both F-NLC and F-P-NLC could reach the posterior segment of the eye, being located mainly in the retina. As already reported in literature the achievement of the posterior segment of the eye could be performed by lipid nanoparticles in a few hours (Balguri et al., 2016; Puglia et al., 2021); in this area, Puglia and coworkers (Puglia et al., 2021) suggested an absorption mechanism for lipid nanoparticles which involves an initial diffusion in the cornea and then the achievement of the retina and the sclera.

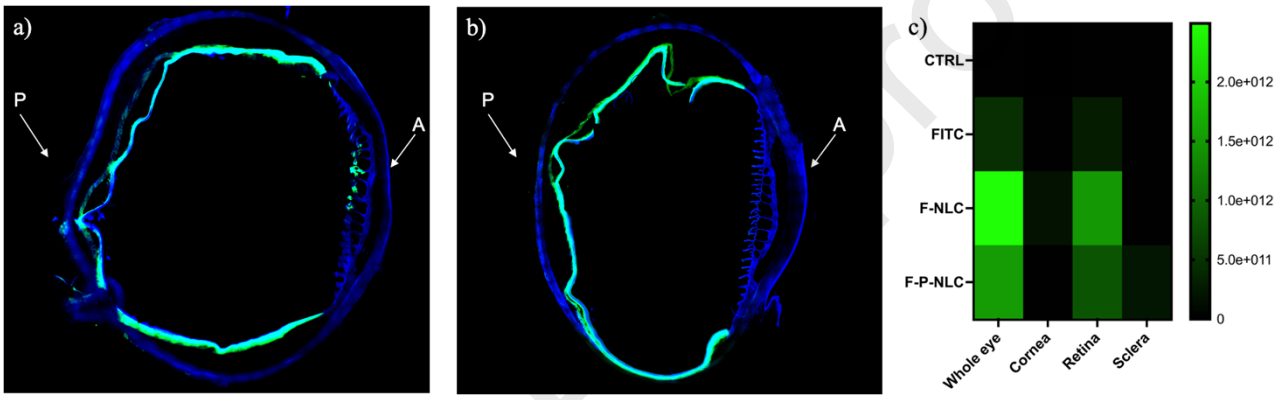

Figure 11. *In vivo* fluorescence images (magnification 5x) of eye after 3 h from the instillation of (**a**) F-NLC and (**b**) F-P-NLC. Anterior (A) and posterior (P) segments are indicated by the arrows; artificial detachment of the retina occurred during sectioning. (**c**) Heat map of average fluorescence intensities of the main ROIs of the eye relatives to the control eye and the eyes treated with free FITC solution, F-NLC and F-P-NLC.

The heat map in Figure 11 c reports the quantification of the fluorescence intensities in the whole eyes as well as in the main regions of interest (ROIs) of the eyes – namely cornea, retina and sclera (Swetledge et al., 2021). These results allowed to make a preliminary comparison between the fluorescence of the two platforms and the probe solution, to highlight the possibility to reach the posterior segment of the eye. Moreover, a higher fluorescence intensity was observed in the eyes treated with the fluorescent nanoparticles, compared to the free FITC solution ones. These results suggest that NLCs initially slightly interact with mucin on the ocular surface – thus reducing the loss caused by tears drainage – then reaching the posterior chamber of the eye. Therefore, after 3 h from the administration, PEGylation did not seem to influence the *in vivo* fate of the nanoparticles, but it resulted advantageous for the enhancement of the anti-inflammatory activity and for the increment of cell viability; moreover, PEG did not alter the mucoadhesion, allowing the nanoparticle to achieve the posterior chamber of the eye. Based on these interesting preliminary results, further studies at different timepoints should be performed to identify the pathway followed by the NLCs to reach the target site.

4. Conclusions

In the present study, a second generation of lipid nanoparticles formulation able to encapsulate a custom-synthetized drug has been developed. The produced NLC and P-NLC samples were produced with optimal features for the intended topical ophthalmic instillation, in terms of particle size, lower than 200 nm, and good homogeneity, confirmed by morphology studies. Therefore, the new synthetized (*S*)-(–)-MRJF22 was successfully encapsulated, demonstrating that the NLC carriers were able to limit the side effects of the antitumoral prodrug, as assessed both *in vitro* and *in vivo*, while enhancing its antiangiogenic and preventive anti-inflammatory activity. Finally, the preliminary *in vivo* biodistribution images obtained after ophthalmic instillation on the fluorescent nanosystems suggested the ability of the carriers to achieve the inner ocular structure, thus promoting drug targeting to choroidal UM.

Declarations of interest: none

Funding

Cinzia Cimino was supported by the PhD program in Biotechnology, XXXVI cycle, University of Catania.

The authors MLG, LB and ESL wish to acknowledge the support of the Spanish Ministry under project PID2021-122187NB-C32 and the support of the Generalitat of Catalonia (2017SGR1447). ESL wants to acknowledge the requalification system grants.

Conflicts of Interest: The authors declare no conflict of interest.

Author contributions

Cinzia Cimino: conceptualization, data curation, formal analysis, investigation, methodology, visualization, writing – original draft, writing – review & editing. **Elena Sánchez López**: investigation, formal analysis, funding acquisition, methodology, supervision, writing – review & editing. **Angela Bonaccorso:** investigation, formal analysis, writing – original draft. **Lorena Bonilla:** investigation, methodology, funding acquisition, writing – review & editing. **Teresa Musumeci:** formal analysis, writing – review & editing. **Josefa Badia:** methodology, resources, writing – review & editing. **Laura Baldomà:** methodology, resources, writing – review & editing. **Rosario Pignatello:** methodology, visualization, writing – review & editing. **Agostino Marrazzo:** resources, writing – review & editing. **Carla Barbaraci:** investigation, writing – review & editing. **María Luisa García:** resources, methodology, funding acquisition, writing – review & editing. **Claudia Carbone:** conceptualization, data curation, funding acquisition, investigation, methodology, resources, project administration, supervision, writing – review & editing.

Acknowledgments

The authors are grateful to NANOMED (Research Centre for Nanomedicine and Pharmaceutical Nanotechnology from the University of Catania) for the technical assistance.

References

Adibkia, K., Shadbad, M.R.S., Nokhodchi, A., Javadzedeh, A., Barzegar-Jalali, M., Barar, J., Mohammadi, G., Omidi, Y., 2007. Piroxicam nanoparticles for ocular delivery: Physicochemical characterization and implementation in endotoxin-induced uveitis. J. Drug Target. 15, 407–416. https://doi.org/10.1080/10611860701453125

Aghaie, T., Jazayeri, M.H., Avan, A., Anissian, A., Salari, A., 2019. Gold nanoparticles and polyethylene glycol alleviate clinical symptoms and alter cytokine secretion in a mouse model of experimental autoimmune encephalomyelitis. IUBMB Life 71, 1313–1321. https://doi.org/10.1002/iub.2045

Aher, S., Singh, R.P., Kumar, M., 2021. Preparation and Characterization of Nano Structured Lipid Carriers for Ocular Bacterial Infection. J. Pharm. Res. Int. 8–23. https://doi.org/10.9734/jpri/2021/v33i40A32215

Ameeduzzafar, Ali, J., Fazil, M., Qumbar, M., Khan, N., Ali, A., 2016. Colloidal drug delivery system: amplify the ocular delivery. Drug Deliv. 23, 700–716. https://doi.org/10.3109/10717544.2014.923065

Anantaworasakul, P., Chaiyana, W., Michniak-Kohn, B.B., Rungseevijitprapa, W., Ampasavate, C., 2020. Enhanced Transdermal Delivery of Concentrated Capsaicin from Chili Extract-Loaded Lipid Nanoparticles with Reduced Skin Irritation. Pharmaceutics 12, 463. https://doi.org/10.3390/pharmaceutics12050463

Balguri, S.P., Adelli, G.R., Majumdar, S., 2016. Topical ophthalmic lipid nanoparticle formulations (SLN, NLC) of indomethacin for delivery to the posterior segment ocular tissues. Eur. J. Pharm. Biopharm. 109, 224–235. https://doi.org/10.1016/j.ejpb.2016.10.015

Barbaraci, C., Giurdanella, G., Leotta, C.G., Longo, A., Amata, E., Dichiara, M., Pasquinucci, L., Turnaturi, R., Prezzavento, O., Cacciatore, I., Zuccarello, E., Lupo, G., Pitari, G.M., Anfuso, C.D., Marrazzo, A., 2021. Haloperidol Metabolite II Valproate Ester (*S*)-(−)-MRJF22: Preliminary Studies as a Potential Multifunctional Agent Against Uveal Melanoma. J. Med. Chem. 64, 13622–13632. https://doi.org/10.1021/acs.jmedchem.1c00995

Bonaccorso, A., Musumeci, T., Carbone, C., Vicari, L., Lauro, M.R., Puglisi, G., 2018. Revisiting the role of sucrose in PLGA-PEG nanocarrier for potential intranasal delivery. Pharm. Dev. Technol. 23, 265–274. https://doi.org/10.1080/10837450.2017.1287731

Bonaccorso, A., Pepe, V., Zappulla, C., Cimino, C., Pricoco, A., Puglisi, G., Giuliano, F., Pignatello, R., Carbone, C., 2021. Sorafenib Repurposing for Ophthalmic Delivery by Lipid Nanoparticles: A Preliminary Study. Pharmaceutics 13, 1956. https://doi.org/10.3390/pharmaceutics13111956

Bonilla, L., Espina, M., Severino, P., Cano, A., Ettcheto, M., Camins, A., García, M.L., Souto, E.B., Sánchez-López, E., 2021. Lipid Nanoparticles for the Posterior Eye Segment. Pharmaceutics 14, 90. https://doi.org/10.3390/pharmaceutics14010090

Bronkhorst, I.H.G., Jager, M.J., 2013. Inflammation in uveal melanoma. Eye 27, 217–223. https://doi.org/10.1038/eye.2012.253

Carbone, C., Caddeo, C., Grimaudo, M.A., Manno, D.E., Serra, A., Musumeci, T., 2020. Ferulic Acid-NLC with Lavandula Essential Oil: A Possible Strategy for Wound-Healing? Nanomaterials 10, 898. https://doi.org/10.3390/nano10050898

Carbone, C., Campisi, A., Manno, D., Serra, A., Spatuzza, M., Musumeci, T., Bonfanti, R., Puglisi, G., 2014a. The critical role of didodecyldimethylammonium bromide on physico-chemical, technological and biological properties of NLC. Colloids Surf. B Biointerfaces 121, 1–10. https://doi.org/10.1016/j.colsurfb.2014.05.024

Carbone, C., Campisi, A., Musumeci, T., Raciti, G., Bonfanti, R., Puglisi, G., 2014b. FA-loaded lipid drug delivery

systems: Preparation, characterization and biological studies. Eur. J. Pharm. Sci. 52, 12–20. https://doi.org/10.1016/j.ejps.2013.10.003

Cimino, C., Leotta, C.G., Marrazzo, A., Musumeci, T., Pitari, G.M., Pignatello, R., Bonaccorso, A., Amata, E., Barbaraci, C., Carbone, C., 2023. Nanostructured lipid carrier for the ophthalmic delivery of haloperidol metabolite II valproate ester (±)-MRJF22: A potential strategy in the treatment of uveal melanoma. J. Drug Deliv. Sci. Technol. 104811. https://doi.org/10.1016/j.jddst.2023.104811

Date, A.A., Srivastava, D., Nagarsenker, M.S., Mulherkar, R., Panicker, L., Aswal, V., Hassan, P.A., Steiniger, F., Thamm, J., Fahr, A., 2011. Lecithin-based novel cationic nanocarriers (LeciPlex) I: fabrication, characterization and evaluation. Nanomed. 6, 1309–1325. https://doi.org/10.2217/nnm.11.38

De Oliveira, I.F., Barbosa, E.J., Peters, M.C.C., Henostroza, M.A.B., Yukuyama, M.N., Dos Santos Neto, E., Löbenberg, R., Bou-Chacra, N., 2020. Cutting-edge advances in therapy for the posterior segment of the eye: Solid lipid nanoparticles and nanostructured lipid carriers. Int. J. Pharm. 589, 119831. https://doi.org/10.1016/j.ijpharm.2020.119831

De Waard-Siebinga, I., Hilders, C.G.J.M., Hansen, B.E., Van Delft, J.L., Jager, M.J., 1996. HLA expression and tumor-infiltrating immune cells in uveal melanoma. Graefes Arch. Clin. Exp. Ophthalmol. 234, 34–42. https://doi.org/10.1007/BF00186516

Delplace, V., Payne, S., Shoichet, M., 2015. Delivery strategies for treatment of age-related ocular diseases: From a biological understanding to biomaterial solutions. J. Controlled Release 219, 652–668. https://doi.org/10.1016/j.jconrel.2015.09.065

Duncan, S.A., Dixit, S., Sahu, R., Martin, D., Baganizi, D.R., Nyairo, E., Villinger, F., Singh, S.R., Dennis, V.A., 2019. Prolonged Release and Functionality of Interleukin-10 Encapsulated within PLA-PEG Nanoparticles. Nanomaterials 9, 1074. https://doi.org/10.3390/nano9081074

Esteruelas, G., Halbaut, L., García-Torra, V., Espina, M., Cano, A., Ettcheto, M., Camins, A., Souto, E.B., Luisa García, M., Sánchez-López, E., 2022. Development and optimization of Riluzole-loaded biodegradable nanoparticles incorporated in a mucoadhesive in situ gel for the posterior eye segment. Int. J. Pharm. 612, 121379. https://doi.org/10.1016/j.ijpharm.2021.121379

Folle, C., Díaz-Garrido, N., Sánchez-López, E., Marqués, A.M., Badia, J., Baldomà, L., Espina, M., Calpena, A.C., García, M.L., 2021a. Surface-Modified Multifunctional Thymol-Loaded Biodegradable Nanoparticles for Topical Acne Treatment. Pharmaceutics 13, 1501. https://doi.org/10.3390/pharmaceutics13091501

Folle, C., Marqués, A.M., Díaz-Garrido, N., Espina, M., Sánchez-López, E., Badia, J., Baldoma, L., Calpena, A.C., García, M.L., 2021b. Thymol-loaded PLGA nanoparticles: an efficient approach for acne treatment. J. Nanobiotechnology 19, 359. https://doi.org/10.1186/s12951-021-01092-z

Grassiri, B., Zambito, Y., Bernkop-Schnürch, A., 2021. Strategies to prolong the residence time of drug delivery systems on ocular surface. Adv. Colloid Interface Sci. 288, 102342. https://doi.org/10.1016/j.cis.2020.102342

Hughes, P., Olejnik, O., Changlin, J., Wilson, C., 2005. Topical and systemic drug delivery to the posterior segments. Adv. Drug Deliv. Rev. 57, 2010–2032. https://doi.org/10.1016/j.addr.2005.09.004

Jokerst, J.V., Lobovkina, T., Zare, R.N., Gambhir, S.S., 2011. Nanoparticle PEGylation for imaging and therapy. Nanomed. 6, 715–728. https://doi.org/10.2217/nnm.11.19

Jounaki, K., Makhmalzadeh, B.S., Feghhi, M., Heidarian, A., 2021. Topical ocular delivery of vancomycin loaded cationic lipid nanocarriers as a promising and non-invasive alternative approach to intravitreal injection for enhanced bacterial endophthalmitis management. Eur. J. Pharm. Sci. 167, 105991. https://doi.org/10.1016/j.ejps.2021.105991

Kakkar, S., Singh, M., Mohan Karuppayil, S., Raut, J.S., Giansanti, F., Papucci, L., Schiavone, N., Nag, T.C., Gao, N., Yu, F.-S.X., Ramzan, M., Kaur, I.P., 2021. Lipo-PEG nano-ocular formulation successfully encapsulates hydrophilic fluconazole and traverses corneal and non-corneal path to reach posterior eye segment. J. Drug Target. 29, 631–650. https://doi.org/10.1080/1061186X.2020.1871483

Karmakar, G., Nahak, P., Guha, P., Roy, B., Nath, R.K., Panda, A.K., 2018. Role of PEG 2000 in the surface modification

766 and physicochemical characteristics of pyrazinamide loaded nanostructured lipid carriers. J. Chem. Sci. 130, 42.
767 https://doi.org/10.1007/s12039-018-1448-x

768 Kiss, E.L., Berkó, S., Gácsi, A., Kovács, A., Katona, G., Soós, J., Csányi, E., Gróf, I., Harazin, A., Deli, M.A., Balogh,
769 G.T., Budai-Szűcs, M., 2020. Development and Characterization of Potential Ocular Mucoadhesive Nano Lipid
770 Carriers Using Full Factorial Design. Pharmaceutics 12, 682. https://doi.org/10.3390/pharmaceutics12070682

771 Kujala, E., Ma¨kitie, T., Kivela¨, T., 2003. Very Long-Term Prognosis of Patients with Malignant Uveal Melanoma.
772 Investig. Opthalmology Vis. Sci. 44, 4651. https://doi.org/10.1167/iovs.03-0538

773 Li, J., Tan, G., Cheng, B., Liu, D., Pan, W., 2017. Transport mechanism of chitosan-N-acetylcysteine, chitosan
774 oligosaccharides or carboxymethyl chitosan decorated coumarin-6 loaded nanostructured lipid carriers across the
775 rabbit ocular. Eur. J. Pharm. Biopharm. 120, 89–97. https://doi.org/10.1016/j.ejpb.2017.08.013

776 Lim, L.T., Ah-Kee, E.Y., Collins, C.E., 2014. Common eye drops and their implications for pH measurements in the
777 management of chemical eye injuries. Int. J. Ophthalmol. 7, 1067–1068. https://doi.org/10.3980/j.issn.2222-
778 3959.2014.06.29

779 Liu, M., Wen, J., Sharma, M., 2020. Solid Lipid Nanoparticles for Topical Drug Delivery: Mechanisms, Dosage Form
780 Perspectives, and Translational Status. Curr. Pharm. Des. 26, 3203–3217.
781 https://doi.org/10.2174/1381612826666200526145706

782 López-Machado, A., Díaz, N., Cano, A., Espina, M., Badía, J., Baldomà, L., Calpena, A.C., Biancardi, M., Souto, E.B.,
783 García, M.L., Sánchez-López, E., 2021. Development of topical eye-drops of lactoferrin-loaded biodegradable
784 nanoparticles for the treatment of anterior segment inflammatory processes. Int. J. Pharm. 609, 121188.
785 https://doi.org/10.1016/j.ijpharm.2021.121188

786 Makoni, P.A., Wa Kasongo, K., Walker, R.B., 2019. Short Term Stability Testing of Efavirenz-Loaded Solid Lipid
787 Nanoparticle (SLN) and Nanostructured Lipid Carrier (NLC) Dispersions. Pharmaceutics 11, 397.
788 https://doi.org/10.3390/pharmaceutics11080397

789 Musumeci, T., Bonaccorso, A., Carbone, C., Russo, G., Pappalardo, F., Puglisi, G., 2019. Design and optimization of
790 PEGylated nanoparticles intended for Berberine Chloride delivery. J. Drug Deliv. Sci. Technol. 52, 521–530.
791 https://doi.org/10.1016/j.jddst.2019.05.012

792 Natarajan, J.V., Chattopadhyay, S., Ang, M., Darwitan, A., Foo, S., Zhen, M., Koo, M., Wong, T.T., Venkatraman, S.S.,
793 2011. Sustained Release of an Anti-Glaucoma Drug: Demonstration of Efficacy of a Liposomal Formulation in the
794 Rabbit Eye. PLoS ONE 6, e24513. https://doi.org/10.1371/journal.pone.0024513

795 Niamprem, P., Srinivas, S.P., Tiyaboonchai, W., 2019. Penetration of Nile red-loaded nanostructured lipid carriers
796 (NLCs) across the porcine cornea. Colloids Surf. B Biointerfaces 176, 371–378.
797 https://doi.org/10.1016/j.colsurfb.2019.01.018

798 Niederkorn, A., Wackernagel, W., Artl, M., Schwantzer, G., Aigner, B., Richtig, E., 2014. Response of patients with
799 metastatic uveal melanoma to combined treatment with fotemustine and sorafenib. Acta Ophthalmol. (Copenh.) 92,
800 e696–e697. https://doi.org/10.1111/aos.12432

801 Nirbhavane, P., Sharma, G., Singh, B., Begum, G., Jones, M.-C., Rauz, S., Vincent, R., Denniston, A.K., Hill, L.J., Katare,
802 O.P., 2020. Triamcinolone acetonide loaded-cationic nano-lipoidal formulation for uveitis: Evidences of improved
803 biopharmaceutical performance and anti-inflammatory activity. Colloids Surf. B Biointerfaces 190, 110902.
804 https://doi.org/10.1016/j.colsurfb.2020.110902

805 Oliveira, A.G.L. de, Silva, R.S., Alves, E.N., Presgrave, R. de F., Presgrave, O.A.F., Delgado, I.F., 2012. Ensaios da
806 membrana cório-alantoide (HET-CAM e CAM-TBS): alternativas para a avaliação toxicológica de produtos com
807 baixo potencial de irritação ocular. Rev. Inst. Adolfo Lutz 71, 153–159. https://doi.org/10.53393/rial.2012.v71.32405

808 Onugwu, A.L., Attama, A.A., Nnamani, P.O., Onugwu, S.O., Onuigbo, E.B., Khutoryanskiy, V.V., 2022. Development
809 and optimization of solid lipid nanoparticles coated with chitosan and poly(2-ethyl-2-oxazoline) for ocular drug
810 delivery of ciprofloxacin. J. Drug Deliv. Sci. Technol. 74, 103527. https://doi.org/10.1016/j.jddst.2022.103527

811 Ortiz, A.C., Yañez, O., Salas-Huenuleo, E., Morales, J.O., 2021. Development of a Nanostructured Lipid Carrier (NLC)

812 by a Low-Energy Method, Comparison of Release Kinetics and Molecular Dynamics Simulation. Pharmaceutics 13,
813 531. https://doi.org/10.3390/pharmaceutics13040531

814 Pignatello, R., 2014. Optimization and Validation of a New Method for the Production of Lipid Nanoparticles for
815 Ophthalmic Application. Int. J. Med. Nano Res. 1. https://doi.org/10.23937/2378-3664/1410006

816 Platania, C.B.M., Dei Cas, M., Cianciolo, S., Fidilio, A., Lazzara, F., Paroni, R., Pignatello, R., Strettoi, E., Ghidoni, R.,
817 Drago, F., Bucolo, C., 2019. Novel ophthalmic formulation of myriocin: implications in retinitis pigmentosa. Drug
818 Deliv. 26, 237–243. https://doi.org/10.1080/10717544.2019.1574936

819 Puglia, C., Santonocito, D., Ostacolo, C., Maria Sommella, E., Campiglia, P., Carbone, C., Drago, F., Pignatello, R.,
820 Bucolo, C., 2020. Ocular Formulation Based on Palmitoylethanolamide-Loaded Nanostructured Lipid Carriers:
821 Technological and Pharmacological Profile. Nanomaterials 10, 287. https://doi.org/10.3390/nano10020287

822 Puglia, C., Santonocito, D., Romeo, G., Intagliata, S., Romano, G.L., Strettoi, E., Novelli, E., Ostacolo, C., Campiglia,
823 P., Sommella, E.M., Pignatello, R., Bucolo, C., 2021. Lipid Nanoparticles Traverse Non-Corneal Path to Reach the
824 Posterior Eye Segment: In Vivo Evidence. Molecules 26, 4673. https://doi.org/10.3390/molecules26154673

825 Rahmi, A., Mammar, H., Thariat, J., Angellier, G., Herault, J., Chauvel, P., Kodjikian, L., Denis, P., Grange, J.D., 2014.
826 Proton beam therapy for presumed and confirmed iris melanomas: a review of 36 cases. Graefes Arch. Clin. Exp.
827 Ophthalmol. 252, 1515–1521. https://doi.org/10.1007/s00417-014-2735-y

828 Razavi, M.S., Ebrahimnejad, P., Fatahi, Y., D'Emanuele, A., Dinarvand, R., 2022. Recent Developments of
829 Nanostructures for the Ocular Delivery of Natural Compounds. Front. Chem. 10, 850757.
830 https://doi.org/10.3389/fchem.2022.850757

831 Sánchez-López, E., Egea, M.A., Cano, A., Espina, M., Calpena, A.C., Ettcheto, M., Camins, A., Souto, E.B., Silva, A.M.,
832 García, M.L., 2016. PEGylated PLGA nanospheres optimized by design of experiments for ocular administration of
833 dexibuprofen—in vitro, ex vivo and in vivo characterization. Colloids Surf. B Biointerfaces 145, 241–250.
834 https://doi.org/10.1016/j.colsurfb.2016.04.054

835 Sánchez-López, E., Espina, M., Doktorovova, S., Souto, E.B., García, M.L., 2017. Lipid nanoparticles (SLN, NLC):
836 Overcoming the anatomical and physiological barriers of the eye – Part I – Barriers and determining factors in ocular
837 delivery. Eur. J. Pharm. Biopharm. 110, 70–75. https://doi.org/10.1016/j.ejpb.2016.10.009

838 Sánchez-López, E., Esteruelas, G., Ortiz, A., Espina, M., Prat, J., Muñoz, M., Cano, A., Calpena, A.C., Ettcheto, M.,
839 Camins, A., Alsafi, Z., Souto, E.B., García, M.L., Pujol, M., 2020. Dexibuprofen Biodegradable Nanoparticles: One
840 Step Closer towards a Better Ocular Interaction Study. Nanomaterials 10, 720. https://doi.org/10.3390/nano10040720

841 Sánchez-López, E., Gómara, M.J., Haro, I., 2023. Atorvastatin-loaded peptide amphiphiles against corneal
842 neovascularization. Nanomed. nnm-2023-0133. https://doi.org/10.2217/nnm-2023-0133

843 Santonocito, D., Sarpietro, M.G., Carbone, C., Panico, A., Campisi, A., Siciliano, E.A., Sposito, G., Castelli, F., Puglia,
844 C., 2020. Curcumin Containing PEGylated Solid Lipid Nanoparticles for Systemic Administration: A Preliminary
845 Study. Molecules 25, 2991. https://doi.org/10.3390/molecules25132991

846 Seftor, E.A., Meltzer, P.S., Kirschmann, D.A., Pe'er, J., Maniotis, A.J., Trent, J.M., Folberg, R., Hendrix, M.J.C., 2002.
847 Molecular determinants of human uveal melanoma invasion and metastasis. Clin. Exp. Metastasis 19, 233–246.
848 https://doi.org/10.1023/A:1015591624171

849 Shen, J., Sun, M., Ping, Q., Ying, Z., Liu, W., 2010. Incorporation of liquid lipid in lipid nanoparticles for ocular drug
850 delivery enhancement. Nanotechnology 21, 025101. https://doi.org/10.1088/0957-4484/21/2/025101

851 Silva, B., São Braz, B., Delgado, E., Gonçalves, L., 2021. Colloidal nanosystems with mucoadhesive properties designed
852 for ocular topical delivery. Int. J. Pharm. 606, 120873. https://doi.org/10.1016/j.ijpharm.2021.120873

853 Spagnolo, F., Caltabiano, G., Queirolo, P., 2012. Uveal melanoma. Cancer Treat. Rev. 38, 549–553.
854 https://doi.org/10.1016/j.ctrv.2012.01.002

855 Swetledge, S., Carter, R., Stout, R., Astete, C.E., Jung, J.P., Sabliov, C.M., 2021. Stability and ocular biodistribution of
856 topically administered PLGA nanoparticles. Sci. Rep. 11, 12270. https://doi.org/10.1038/s41598-021-90792-5

Tambe, S., Jain, D., Amin, P., 2021. Simultaneous determination of dorzolamide and timolol by first-order derivative UV spectroscopy in simulated biological fluid for in vitro drug release testing. Spectrochim. Acta. A. Mol. Biomol. Spectrosc. 255, 119682. https://doi.org/10.1016/j.saa.2021.119682

Thrimawithana, T.R., Young, S., Bunt, C.R., Green, C., Alany, R.G., 2011. Drug delivery to the posterior segment of the eye. Drug Discov. Today 16, 270–277. https://doi.org/10.1016/j.drudis.2010.12.004

Urtti, A., 2006. Challenges and obstacles of ocular pharmacokinetics and drug delivery. Adv. Drug Deliv. Rev. 58, 1131–1135. https://doi.org/10.1016/j.addr.2006.07.027

Varela-Fernández, R., García-Otero, X., Díaz-Tomé, V., Regueiro, U., López-López, M., González-Barcia, M., Isabel Lema, M., Javier Otero-Espinar, F., 2022. Lactoferrin-loaded nanostructured lipid carriers (NLCs) as a new formulation for optimized ocular drug delivery. Eur. J. Pharm. Biopharm. 172, 144–156. https://doi.org/10.1016/j.ejpb.2022.02.010

Vega, E., Egea, M.A., Valls, O., Espina, M., García, M.L., 2006. Flurbiprofen Loaded Biodegradable Nanoparticles for Ophtalmic Administration. J. Pharm. Sci. 95, 2393–2405. https://doi.org/10.1002/jps.20685

Viegas, C., Patrício, A.B., Prata, J.M., Nadhman, A., Chintamaneni, P.K., Fonte, P., 2023. Solid Lipid Nanoparticles vs. Nanostructured Lipid Carriers: A Comparative Review. Pharmaceutics 15, 1593. https://doi.org/10.3390/pharmaceutics15061593

Highlights:

1. NLCs with adequate features for ocular administration were designed and prepared.
2. Prodrug encapsulation into NLCs protects the cornea from irritative side effect.
3. Antiangiogenic assay confirmed the antitumoral activity of the loaded NLCs.
4. Loaded NLCs were able to prevent ocular inflammation *in vivo*.
5. Preliminary fluorescence images suggested NLCs ability to reach the inner eye.